Calculations with FS2R code of 6 nm and 70 nm Options of SASE FEL at the TESLA Test Facility

E.L. Saldin, E.A. Schneidmiller

Automatic Systems Corporation, 443050 Samara, Russia

M.V. Yurkov

Joint Institute for Nuclear Research, Dubna, 141980 Moscow Region, Russia

Abstract

This paper presents brief description of the collection of computer codes FS2R for calculations of an FEL amplifier with an axisymmetric electron beam. Program package FS2R includes the following routines:

– Program FS2RD allows one to analyze eigenvalue problem (i.e. to find increments, field distributions in Fresnel diffraction zone and directivity diagrams in Fraunhofer diffraction zone) for the cases of the electron beam with stepped (analytical solution), bounded parabolic (analytical solution) and arbitrary gradient profile of current density (multilayer approximation method). All the solutions are obtained taking into account diffraction effects, space charge fields and energy spread of electrons in the beam.

– Program FS2RL allows one to solve initial problem, i.e. to find in the linear approximation the evolution of the electromagnetic field in the FEL amplifier at given initial conditions at the undulator entrance. In the case of the stepped profile of the electron beam current density the eigenvalue problem is solved analytically and in the case of an arbitrary profile it is solved by direct integration of the self-consistent field equations.

– Program FS2RN is nonlinear simulation code.

Programs of the FS2R package are used for calculations of the parameters of SASE FEL which is being planned to construct at the TESLA Test Facility at DESY.

5 June 1995

1 Introduction

R&D works on future generation linear colliders give a promise to obtain in the nearest future high-energy, low-emittance and monochromatic electron beams which could be used for a wide range of applications. One of the possible applications of these beams, which is under study at DESY and SLAC, is to use them as driving beams for SASE FEL (self amplified spontaneous emission free electron laser). Special improvement of a quality of the electron beam from SLAC accelerator will allow, in principle, to construct SASE FEL operating in soft X-ray range [1].

Project parameters of the TESLA Test Facility accelerator are rather promising to use it as driving accelerator for SASE FEL [2]. Installation of bunch compressors to decrease bunch length and to increase peak current could made such a possibility to be realistic.

One of the problems of the SASE FEL design consists in calculation of the output characteristics of such an FEL amplifier. To realize this we should remember distinctions between SASE FEL and traditional FEL amplifier. Traditional FEL amplifier amplifies electromagnetic radiation generated by master oscillator. The amplitude and frequency of the input signal is controlled by experimenter. As a rule, the signal of master oscillator has narrow bandwidth. Under these initial conditions the field amplitude in the undulator does not depend on time and depends only on coordinates. This was the main factor which has allowed to develop a wide range of reliable theoretical approaches for calculation of characteristics of traditional FEL amplifier [3] - [13]. These are, so called, steady-state models of the FEL amplifier.

Contrary to traditional FEL amplifier, situation with the SASE FEL is more complicated. It is connected with the fact that fluctuations of the beam current density play role of the input signal. First, these fluctuations vary in time. Second, a spectrum of these fluctuations is "white". To be strict, to describe such a situation, three-dimensional time-dependent theory of the FEL amplifier should be developed.

Nevertheless, theoretical approach developed for description of traditional FEL amplifiers could be used to find some characteristics of the SASE FEL. First of all, such an approach allows one to calculate rather rigorously characteristics of the radiation modes of the SASE FEL. This is consequence of the fact that "effective" power of the input signal in the SASE FEL is rather small with respect to the saturation power. As a result, the only mode is survived having maximal increment. Characteristics of this mode do not depend on the nature of input signal and are determined with parameters of the FEL amplifier. So, the results of the steady-state theory allows one to calculate increments, field distributions in Fresnel zone (i.e. inside the undulator) and directivity diagrams of radiation power in Fraunhofer diffraction zone (i.e. in experimental area). These are rigorous results which do not depend on initial conditions at the amplifier entrance. Calculations of the frequency characteristic of the

FEL amplifier allows one to estimate rather rigorously the bandwidth of the SASE FEL. Calculation of the amplitude characteristic of the FEL amplifier allows one to estimate influence of the fluctuations of the input amplitude on the output amplitude.

The paper is organized as follows. In sections 2 – 4 we present the basis of the theory of the FEL amplifier with an axisymmetric electron beam [11–13]. Our approach allows one to take into account diffraction effects, energy spread of the electrons in the beam and space charge effects. On the base of this theory we have developed program package FS2R for calculations of the FEL amplifier. The package consists of three programs: FS2RD, FS2RL and FS2RN. Program FS2RD allows one to perform analysis of the eigenvalue problem (finding eigenvalues (increments) of the radiation modes and field distributions in Fresnel and Fraunhofer diffraction zones). This program is essentially based on analytical techniques developed in refs. [11,13]. Program FS2RL allows one to calculate evolution of the electromagnetic field amplitude in the linear mode of the FEL amplifier operation. In the case of a stepped profile of the beam current density the code essentially use analytical techniques and in the case of an arbitrary gradient profile of the beam current density we use method of direct integration of the self-consistent field equations. Program FS2RN is numerical simulation code and allows one to calculate characteristics of the FEL amplifier operating in the nonlinear mode.

In section 5 we present physical estimation of the "effective" power of shot noise at the FEL amplifier entrance.

In section 6 we use the programs of the FS2R package to calculate various characteristics of the FEL amplifier (6 nm and 70 nm options). On the base of these calculations we predict characteristics of the SASE FEL which is designed at the TESLA Test Facility. We calculate increments of the radiation modes, field distributions inside the undulator and in experimental area and bandwidth of the SASE FEL. We also study the influence of the emittance, energy spread and deviation of the beam current off nominal value on the FEL amplifier operation. On the base of these calculations we can estimate also the required length of the undulator.

2 Basic equations

The analyzed model is based on the Maxwell's wave equations taken in the paraxial approximation and the description of the electron beam with the kinetic equation expressed in "energy-phase" variables. It is anticipated that electrons move (on the average over constrained motion) only along the trajectories parallel to the undulator axis. Such a model has proved to be very fruitful to describe the physical phenomena in the FEL amplifiers and allows one to take into consideration such effects as diffraction of radiation, space charge fields and energy spread of electrons in the beam.

2.1 Effective Hamiltonian

Let us consider an FEL amplifier with a helical undulator. The undulator magnetic field at the axis has the form:

$$\vec{H}_w(z) = \vec{e}_x H_w \cos(\kappa_w z) - \vec{e}_y H_w \sin(\kappa_w z), \tag{2.1}$$

where $\kappa_w = 2\pi/\lambda_w$ is the undulator wavenumber and $\vec{e}_{x,y}$ are unit vectors directed along the x and y axes of the Cartesian coordinate system (x, y, z). We neglect the transverse variation of the magnetic field and assume the electrons to move along the constrained helical trajectories parallel to the z axis. The electron rotation angle $\theta_s = K/\gamma$ (where $\gamma = \mathcal{E}_0/m_e c^2$ is relativistic factor of the electron with nominal energy $\mathcal{E}_0$, $K = eH_w/m_e c^2 \kappa_w$ is undulator parameter, $(-e)$ and m_e are the charge and the mass of the electron, respectively, and c is the velocity of light) is considered to be small and the longitudinal electron velocity v_z is close to the velocity of light c ($v_z \simeq c$).

The electric field of the amplified wave is presented in the complex form:

$$E_x + iE_y = \tilde{E}(z, \vec{r}_\perp) \exp[i\omega(z/c - t)], \tag{2.2}$$

where ω is the frequency of the amplified wave. The complex amplitude of the field $\tilde{E}$ does not depend on time at any space point which corresponds to the standard formulation of the initial problem with the definite initial conditions at the undulator entrance at $z = 0$. We assume the complex amplitude $\tilde{E}(z, \vec{r}_\perp)$ to be a slowly changing function, i.e. $\mid \partial\tilde{E}/\partial z \mid \ll \kappa_w \mid \tilde{E} \mid$.

We describe the motion of the electrons using "energy-phase" variables with the phase $\psi = \kappa_w z + \omega(z/c - t)$ as canonical coordinate and $\mathcal{P} = \mathcal{E}/\omega$ as canonical momentum. In this representation coordinate z is independent variable. When transverse motion of the particles is defined by the undulator field ant not with the radiation field, i.e. $\mid \tilde{E} \mid (1 - v_z/c) \ll H_w$, hamiltonian is of the form [13]:

$$\tilde{\mathcal{H}} = \frac{\mathcal{E}}{\omega}(\kappa_w + \omega/c) - \frac{1}{c}\left[\mathcal{E}^2 - e^2 \mid \vec{A}_w \mid^2 - m_e^2 c^4\right]^{1/2} + \frac{e^2(\vec{A}\cdot\vec{A}_w)}{c}\left[\mathcal{E}^2 - e^2 \mid \vec{A}_w \mid^2 - m_e^2 c^4\right]^{-1/2} + \frac{e}{\omega}\int d\psi E_z. \tag{2.3}$$

Here $\vec{A}_w(z) = -\vec{e}_z \times \int \vec{H}_w dz$ is vector potential of the undulator field, $\vec{A}$ is vector potential of the electromagnetic wave ($\vec{E} = c^{-1}\partial\vec{A}/\partial t$) and E_z is longitudinal component of the space charge field.

The canonical equations of motion have the form

$$d\psi/dz = \partial\tilde{\mathcal{H}}/\partial\mathcal{P},$$
$$d\mathcal{P}/dz = -\partial\tilde{\mathcal{H}}/\partial\psi. \tag{2.4}$$

At small deviations of the electron energy $\mathcal{E}$ from the nominal one $\mathcal{E}_0$, hamiltonian (2.3) takes the form:

$$\tilde{\mathcal{H}}\omega = H(P,\psi,z) = CP + \frac{\omega}{2c\gamma_z^2\mathcal{E}_0}P^2 - \left(Ue^{i\psi} + U^*e^{-i\psi}\right)\left(1 - P/\mathcal{E}_0\right) + \int d\psi e E_z, \tag{2.5}$$

where $P = \mathcal{E} - \mathcal{E}_0$, $C = \kappa_w - \omega/(2c\gamma_z^2)$ is the detuning of the electron with the nominal energy $\mathcal{E}_0$, $U = -e\theta_s\tilde{E}(z,\vec{r}_\perp)/(2i)$ is the complex amplitude of the effective potential of the particle interaction with the electromagnetic wave, and

$$\theta_s = eH_w/(\mathcal{E}_0\kappa_w), \qquad \gamma_z^{-2} = \gamma^{-2} + \theta_s^2, \qquad \gamma = \mathcal{E}_0/(m_ec^2).$$

2.2 Self-consistent equations of the linear theory

In exposing the linear theory the main emphasis is put on finding analytic solutions of the self-consistent field equations. An interaction process of the electron beam with electromagnetic wave in an undulator in the linear mode of operation can be described by a unique integro-differential equation. The solution of the latter under stated initial conditions at the entrance into the interaction region allows to determine a relationship between wave field amplitude and undulator length and thus to calculate the output characteristics of the FEL amplifier. These analytic solutions serve as a reliable basis for the development of numerical methods. The analysis of nonlinear processes refers to the problems solvable only numerically by a computer. On the other hand, testing of the numerical simulation codes would be difficult without the use of rigorous results of the FEL amplifier linear theory as a primary standard.

To obtain general form of self-consistent equations of linear theory, we use the following approximations:

a) electrons move only in the z direction,
b) complex amplitude of the electric field $\tilde{E}$ is the slowly changing function, i.e. $|\,\partial\tilde{E}/\partial z\,| \ll \kappa_w\,|\,\tilde{E}\,|$;
c) the transverse electron beam dimension is rather large, i.e. $r_b^2 \gg \gamma_z^2c^2/\omega^2$;
d) the electron beam at the undulator entrance is modulated neither in velocity nor

density.

These approximations allow us to derive from kinetic equation and Maxwell's equations the self-consistent field equations describing the linear mode of the FEL amplifier operation. These equations could be written as for the field amplitude as well as for the first harmonic of the beam current density. The corresponding equation for the amplitude of the electromagnetic field has the form [11]:

$$\nabla_\perp^2 \tilde{E} + 2i\frac{\omega}{c}\frac{\partial \tilde{E}}{\partial z} = ij_0(\vec{r}_\perp)\int_0^z dz' \left[\frac{2\pi e}{c^2}\theta_s^2\omega\tilde{E}(z',\vec{r}_\perp) + \frac{4\pi e}{\omega}\left[\nabla_\perp^2\tilde{E} + 2i\frac{\omega}{c}\frac{\partial\tilde{E}}{\partial z'}\right]\right]\times \int_{-\infty}^{\infty} dP\frac{dF}{dP}\exp\left[i\left(C + \frac{\omega}{\gamma_z^2\mathcal{E}_0 c}P\right)(z'-z)\right], \tag{2.6}$$

where $F(P)$ is the function describing the energy distribution and is normalized to the unity.

The corresponding integral equation for the first harmonic of the beam current density $\tilde{j}_1(z,\vec{r}_\perp)$ [1] has the form [11]:

$$\tilde{j}_1(z,\vec{r}_\perp) = ij_0(\vec{r}_\perp)\int_0^z dz'\left\{-\frac{e\theta_s}{2i}\tilde{E}_{\text{ext}}(z',\vec{r}_\perp) + \frac{4\pi e}{\omega}\tilde{j}_1(z',\vec{r}_\perp) - \frac{e\theta_s^2\omega}{2c^2}\int_0^{z'}\frac{dz''}{z'-z''}\int d\vec{r}'_\perp\tilde{j}_1(z'',\vec{r}'_\perp)\exp\left[\frac{i\omega\mid\vec{r}_\perp-\vec{r}'_\perp\mid^2}{2c(z'-z'')}\right]\right\}\times \int_{-\infty}^{\infty} dP\frac{dF}{dP}\exp\left[i\left(C+\frac{\omega}{\gamma_z^2\mathcal{E}_0 c}P\right)(z'-z)\right]. \tag{2.7}$$

When the energy spread is negligibly small ($F(P) \to \delta(P)$, where $\delta(P)$ is the delta function), this equation is reduced to:

$$\frac{d^2\tilde{j}_1}{dz^2} + 2iC\frac{d\tilde{j}_1}{dz} + \left[\frac{4\pi e}{c\gamma_z^2\mathcal{E}_0}j_0(\vec{r}_\perp) - C^2\right]\tilde{j}_1 = \frac{\omega}{c\gamma_z^2\mathcal{E}_0}j_0(\vec{r}_\perp)\left\{\frac{e\theta_s}{2i}\tilde{E}_{\text{ext}}(z,\vec{r}_\perp) + \frac{e\theta_s^2\omega}{2c^2}\int_0^z\frac{dz'}{z-z'}\int d\vec{r}'_\perp\tilde{j}_1(z',\vec{r}'_\perp)\times\right.$$

[1] $j_z = -j_0(\vec{r}_\perp) + \tilde{j}_1\exp^{i\psi} + C.C.$

$$\exp\left[\frac{i\omega \mid \vec{r}_\perp - \vec{r}'_\perp \mid^2}{2c(z-z')}\right]\Bigg\}. \tag{2.8}$$

So, the self-consistent field method in the linear approximation enables one to get from the kinetic equation and Maxwell's equations the only equation either for the field amplitude of amplified wave (2.6) or for the modulation amplitude of the beam current density (2.7). Both of the ways lead to the same results but for the analytical calculations it is preferable to use the equation for the wave field: in this case the mathematical apparatus is always connected with more conventional differential equations. At the same time the situations with the computer simulations is proved to be reversed and the method using the equation for the modulation amplitude of the beam current density is more convenient.

2.3 Self-consistent equations of the nonlinear theory

The analysis of nonlinear processes refers to the problems solvable only numerically by a computer. We use standard approach for constructing numerical algorithm for the FEL amplifier operation. We simulate the real particles of the beam with a finite number of macroparticles which move in the given electromagnetic field in accordance with the canonical equations of motion (2.4). Then we calculate the current and the charge density produced by these macroparticles and find electromagnetic fields from Maxwell's equations thus providing self-consistent solution of the problem .

3 Linear theory of the FEL amplifier with an axisymmetric electron beam

In this section we present brief description of analytical and numerical techniques implemented in the programs FS2RD and FS2RL to calculate the linear mode of operation of the FEL amplifier with an axisymmetric electron beam. An FEL model is used wherein diffraction effects, space charge fields and energy spread of electrons in the beam are taken into account. We have shown in section 2 that in the linear approximation the self-consistent field method makes possible to get from the kinetic and Maxwell's equations the only integro-differential equation for the radiation field amplitude. We use this equation to solve the eigenvalue problem. To find the eigenvalues and eigenfunctions we use the condition of the quadratic integrability of the eigenfunction and the continuity conditions of the eigenfunction and its derivative at the beam boundary. The obtained solutions allow one to calculate increments of the eigenmodes, find the field distributions in the Fresnel and Fraunhofer diffraction zones.

The next problem of the linear theory is the initial-value problem consisting in the finding of the evolution of the amplified wave under given conditions at the undulator

entrance. We solve the initial problem for the practically important case with the unmodulated electron beam and electromagnetic radiation from the master oscillator at the entrance into the undulator. When the electron beam profile is stepped, the initial problem is solved analytically with the Laplace transform technique. The asymptotic formulae for the high gain limit are derived taking into account diffraction of radiation, space charge fields and energy spread of the electrons in the beam. When the electron beam has the arbitrary gradient profile there is no possibility to obtain the rigorous analytical solution of the initial problem. For this case we have developed the algorithm of numerical integration of the self-consistent field equations.

We consider two profiles of the beam current density:

bounded gradient profile:

$$j(r) = \begin{cases} IS(r/r_0)\left[2\pi \int\limits_0^{r_0} rS(r/r_0)dr\right]^{-1} & \text{at} \quad r < r_0, \\ 0 & \text{at} \quad r > r_0, \end{cases} \tag{3.1a}$$

(here I is the beam current, $S(r/r_0)$ is the function describing the gradient profile and r_0 is radius of the beam);

gaussian profile:

$$j(r) = \frac{I}{2\pi\sigma_r^2}\exp(-r^2/2\sigma_r^2), \tag{3.1b}$$

where σ_r is the width of the gaussian distribution.

3.1 Solution of the eigenvalue problem

Let us consider the electron beam with the bounded gradient profile of the beam current density given by eq. (3.1a). Using polar coordinates (r, φ, z), in the high-gain limit we shall seek the solution of eq. (2.6) in the form:

$$\tilde{E}(z, r, \varphi) = \Phi_n(r)e^{\Lambda z}\begin{pmatrix} \cos(n\varphi) \\ \sin(n\varphi) \end{pmatrix}, \tag{3.2}$$

where n is integer, $n \geq 0$. Substituting expressions (3.2) into eq. (2.6) we get:

Region 1, ($\hat{r} < 1$):

$$\left[\frac{d^2}{d\hat{r}^2} + \frac{1}{\hat{r}}\frac{d}{d\hat{r}} - \frac{2i\hat{D}S(\hat{r})}{1 - i\hat{\Lambda}_p^2\hat{D}S(\hat{r})} - \frac{n^2}{\hat{r}^2} + 2iB\hat{\Lambda}\right]\Phi_n(\hat{r}) = 0, \tag{3.3a}$$

Region 2, ($\hat{r} > 1$):

$$\left[\frac{d^2}{d\hat{r}^2} + \frac{1}{\hat{r}}\frac{d}{d\hat{r}} - \frac{n^2}{\hat{r}^2} + 2iB\hat{\Lambda}\right]\Phi_n(\hat{r}) = 0, \tag{3.3b}$$

where the following notations have been introduced:

$$\begin{aligned}
&\hat{z} = \Gamma z, \qquad \hat{r} = r/r_0, \qquad \hat{\Lambda} = \Lambda/\Gamma, \qquad \hat{C} = C/\Gamma, \\
&\hat{\Lambda}_p^2 = 4c^2(\theta_s r_0\omega)^{-2}, \qquad \hat{\Lambda}_T^2 = \Lambda_T^2/\Gamma^2, \qquad B = \Gamma r_0^2\omega/c, \\
&\Lambda_T^2 = <(\Delta\mathcal{E})^2>\omega^2/(c^2\gamma_z^4\mathcal{E}_0^2) \\
&\Gamma = \left[I\omega^2\theta_s^2\left(2I_A c^2\gamma_z^2\gamma\int_0^1 \xi S(\xi)d\xi\right)^{-1}\right]^{1/2}, \\
&\hat{D} = i\int_0^\infty \exp\left[-\hat{\Lambda}_T^2\xi^2/2 - \left(\hat{\Lambda} + i\hat{C}\right)\right]\xi d\xi.
\end{aligned} \tag{3.4}$$

For definiteness we assume the energy spread of the electrons in the beam to be gaussian.

In the case of stepped and bounded parabolic profile of the beam current density eqs. (3.3) could be solved analytically. In the case of an arbitrary profile of the beam current density the eigenvalue problem is solved semi-analytically with application of multilayer approximation method.

3.1.1 Stepped profile

Let us consider the homogeneous axisymmetric electron beam with radius r_0 ($S(r/r_0) = 1$ in eq. (3.1a)). In this case equations (3.3) are Bessel equations:

$$\hat{r}^2 d^2\Phi_n/d\hat{r}^2 + \hat{r}d\Phi_n/d\hat{r} + (\mu^2\hat{r}^2 - n^2)\Phi_n = 0 \qquad \text{at } \hat{r} < 1, \tag{3.5a}$$

$$\hat{r}^2 d^2\Phi_n/d\hat{r}^2 + \hat{r}d\Phi_n/d\hat{r} - (g^2\hat{r}^2 + n^2)\Phi_n = 0, \qquad \text{at } \hat{r} > 1, \tag{3.5b}$$

where

$$\mu^2 = \frac{-2i\hat{D}}{1 - i\hat{\Lambda}_p^2\hat{D}} - g^2, \qquad g^2 = -2iB\hat{\Lambda}.$$

To avoid the singularity at $\hat{r} = 0$ the solution for $\Phi_n(\hat{r})$ inside the beam should be chosen in the form:

$$\Phi_n(\hat{r}) = C_1 J_n(\mu\hat{r}), \qquad \text{at } \hat{r} < 1,$$

where J_n is the Bessel function of the first kind of order n. As the field must vanish at $r \to \infty$, we should choose the solution for $\Phi_n(\hat{r})$ outside the beam in the form (we assume here that $\mathrm{Re}(g) > 0$):

$$\Phi_n(\hat{r}) = C_2 K_n(g\hat{r}), \qquad \text{at } \hat{r} > 1,$$

where K_n is the modified Bessel function. The continuity conditions of Φ_n and $d\Phi_n/d\hat{r}$ at the beam boundary give us the eigenvalue equation for the FEL amplifier with the homogeneous axisymmetric electron beam:

$$\mu J_{n+1}(\mu)K_n(g) = gJ_n(\mu)K_{n+1}(g). \tag{3.6}$$

The field mode eigenfunction (i.e. transverse field distribution inside the undulator) is given with the expressions:

$$\Phi_n(\hat{r}) = \begin{cases} J_n(\mu\hat{r}), & \text{at } \hat{r} < 1 \\ J_n(\mu)K_n(g\hat{r})/K_n(g), & \text{at } \hat{r} > 1. \end{cases} \tag{3.7}$$

The directivity diagram of the radiation intensity is one of the important characteristics of FEL amplifier. At large distance from the amplifier exit, at $z \gg l_w$, the output radiation has the form of a spherical wave. In the axisymmetric case the radiation field amplitude depends on the observation angle $\theta = r/z$ according to the expression (we assume here the Fraunhofer diffraction approximation):

$$\Xi(\hat{\theta}) = \int_0^\infty \Phi_0(\hat{r})J_0(\hat{\theta}\hat{r})\hat{r}\,d\hat{r}, \tag{3.8}$$

where $\hat{\theta} = \theta r_0\omega/c$ is the reduced observation angle, $\Phi_0(\hat{r})$ is the complex amplitude of axisymmetric radiation mode at the amplifier output and J_0 is the Bessel function

of the first kind. When the FEL amplifier operates at the ground TEM_{00} mode, using eq. (3.7) we can write the following expression for $\Xi(\theta)$:

$$\Xi(\hat{\theta}) = \int_0^1 \zeta J_0(\hat{\theta}\zeta) J_0(\mu\zeta) d\zeta + \int_1^\infty d\zeta J_0(\mu) J_0(\hat{\theta}\zeta) K_0(g\zeta)/K_0(g) =$$
$$\frac{1}{\hat{\theta}^2-\mu^2}\left[\hat{\theta} J_0(\mu) J_1(\hat{\theta}) - \mu J_1(\mu) J_0(\hat{\theta})\right] -$$
$$\frac{1}{g^2+\hat{\theta}^2}\left[\hat{\theta} J_1(\hat{\theta}) J_0(\mu) - g J_0(\hat{\theta}) J_0(\mu) K_1(g)/K_0(g)\right].$$

Taking into account equation (3.6) we get the following expression for the radiation power directivity diagram:

$$\frac{I(\hat{\theta})}{I(0)} = \left|\frac{\Xi(\hat{\theta})}{\Xi(0)}\right|^2 = \left|\frac{J_0(\hat{\theta}) - \hat{\theta} J_1(\hat{\theta}) J_0(\mu) K_1(g)/K_0(g)}{(1+\hat{\theta}^2/g^2)(1-\hat{\theta}^2/\mu^2)}\right|^2. \tag{3.9}$$

At large values of the diffraction parameter B the Fraunhofer diffraction approximation may be used when $cR_i/(r_0^2\omega) \gg 1$, where R_i is the distance between the observation point and the amplifier exit. When $B \lesssim 1$ the above condition changes to: $\mid \Lambda \mid R_i \simeq \Gamma R_i \gg 1$.

3.1.2 Bounded parabolic profile

The bounded parabolic profile is given with the function $S(\hat{r}) = 1 - k_1^2\hat{r}^2$ in eq. (3.1a), where $k_1 \geq 1$. As far as we know, this is the only gradient profile allowing analytical solution of eq. (3.3a) in the limit of $\hat{\Lambda}_p^2 \to 0$. Introducing notations

$$\mu^2 = -2i\hat{D} - g^2, \qquad g^2 = -2iB\hat{\Lambda}, \qquad \delta^2 = -2\hat{D}k_1^2, \tag{3.10}$$

we rewrite equation (3.3a) in the following standard form:

$$\frac{d^2}{d\hat{r}^2}\Phi_n(\hat{r}) + \frac{1}{\hat{r}}\frac{d}{d\hat{r}}\Phi_n(\hat{r}) + \left[\mu^2 - \delta^2\hat{r}^2 - \frac{n^2}{\hat{r}^2}\right]\Phi_n(\hat{r}) = 0. \tag{3.11}$$

General solution of eq. (3.11) has the form:

$$\Phi_n(\hat{r}) = C_1\hat{r}^n \exp(-\delta\hat{r}^2/2)\,{}_1F_1(\epsilon, n+1, \delta\hat{r}^2) \qquad \text{at } \hat{r} < 1,$$

where ${}_1F_1$ is confluent hypergeometric function and

$$\epsilon = (n+1)/2 - \mu^2/(4\delta).$$

Differential equation (3.3b) is Bessel equation, so the solution for Φ_n outside the beam has the form ($\mathrm{Re}(g) > 0$):

$$\Phi_n(\hat{r}) = C_2 K_n(g\hat{r})\text{at} \qquad \hat{r} > 1,$$

where $g^2 = -2iB\hat{\Lambda}$, $\mathrm{Re}(g) > 0$. Using continuity conditions of Φ_n and $d\Phi_n/d\hat{r}$ at the beam boundary, we obtain the following eigenvalue equation:

$$\delta K_n(g)\left[\frac{2\epsilon}{n+1}{}_1F_1(\epsilon+1, n+2, \delta) - {}_1F_1(\epsilon, n+1, \delta)\right] + gK_{n+1}(g){}_1F_1(\epsilon, n+1, \delta) = 0. \tag{3.12}$$

Eigenfunction of the radiation mode is given with expressions:

$$\Phi_n(\hat{(}r) = \begin{cases} \hat{r}^n \exp(-\delta\hat{r}^2/2){}_1F_1(\epsilon, n+1, \delta\hat{r}^2) & \text{at } r < r_0 \\ \exp(-\delta/2){}_1F_1(\epsilon, n+1, \delta)K_n(g\hat{r})/K_n(g) & \text{at } r < r_0. \end{cases} \tag{3.13}$$

3.1.3 Arbitrary bounded gradient profile

The approach presented above can be easily extended to the case of the electron beam with an arbitrary gradient profile of current density. It can be performed by means of multilayer approximation method. The similar method is used, for example, in the optical waveguide theory (see ref. [15]). This method consists in replacing the electron beam profile with a set of layers and in each of them the current density is supposed to be constant. The fulfillment of the continuity conditions of the eigenfunction and its derivative at all boundaries between the layers leads to the eigenvalue equation (see refs. [11,16,17] for more details).

Let us divide region $0 < \hat{r} < 1$ into K equal parts and assume the beam current density to be constant within each layer. Solution of eq. (3.3a) in each layer has the form:

$$\Phi_n^{(j)} = A_j J_n(\mu_j\hat{r}) + D_j N_n(\mu_j\hat{r}),$$

where $(j-1)/K < \hat{r} < j/K$, A_j and D_j are constants, J_n and N_n are Bessel function of the first and the second kind of order n. Parameters μ_j are given with

$$\mu_j^2 = -2i\hat{D}S_{j-1/2}\left(1 - i\hat{\Lambda}_p^2\hat{D}S_{j-1/2}\right)^{-1} - g^2, \qquad g^2 = -2iB\hat{\Lambda},$$

where $S_{j-1/2} = S(\hat{r}_{j-1/2})$ and $\hat{r}_{j-1/2} = (j-1/2)/K$. To avoid singularity of the solution at $\hat{r} = 0$, we should let $D_1 = 0$. Coefficients A_{j+1} and D_{j+1} are connected

with coefficients A_j and D_j via the continuity conditions of Φ_n and $d\Phi_n/d\hat{r}$ at the boundaries between layers:

$$\begin{pmatrix} A_{j+1} \\ D_{j+1} \end{pmatrix} = T_j \begin{pmatrix} A_j \\ D_j \end{pmatrix}, \qquad j = 1, 2, \ldots, K-1, \tag{3.14}$$

where elements of matrix T_j are given with expression ($\hat{r}_j = j/K$):

$$(T_j)_{11} = \frac{\pi}{2}\hat{r}_j \left[\mu_j J_m(\mu_j \hat{r}_j) N_{m-1}(\mu_{j+1}\hat{r}_j) - \mu_{j+1} J_{m-1}(\mu_j \hat{r}_j) N_m(\mu_{j+1}\hat{r}_j)\right],$$

$$(T_j)_{12} = \frac{\pi}{2}\hat{r}_j \left[\mu_j N_m(\mu_j \hat{r}_j) N_{m-1}(\mu_{j+1}\hat{r}_j) - \mu_{j+1} N_{m-1}(\mu_j \hat{r}_j) N_m(\mu_{j+1}\hat{r}_j)\right],$$

$$(T_j)_{21} = -\frac{\pi}{2}\hat{r}_j \left[\mu_j J_m(\mu_j \hat{r}_j) J_{m-1}(\mu_{j+1}\hat{r}_j) - \mu_{j+1} J_{m-1}(\mu_j \hat{r}_j) J_m(\mu_{j+1}\hat{r}_j)\right],$$

$$(T_j)_{22} = -\frac{\pi}{2}\hat{r}_j \left[\mu_j N_m(\mu_j \hat{r}_j) J_{m-1}(\mu_{j+1}\hat{r}_j) - \mu_{j+1} N_{m-1}(\mu_j \hat{r}_j) J_m(\mu_{j+1}\hat{r}_j)\right].$$

In the region outside the electron beam, solution of eq. (3.3b) satisfying the quadratic integrability condition has the form $\Phi = F_1 K_n(g\hat{r}), \mathrm{Re}(g) > 0$. At the boundary of the last layer, at $\hat{r} = 1$, the continuity conditions of Φ_n and $d\Phi_n/d\hat{r}$ at the boundary leads to relations:

$$A_K J_n(\mu_K) + D_K N_n(\mu_K) = F_1 K_n(g),$$

$$\mu_K A_K J_{n+1}(\mu_K) + \mu_K D_K N_{n+1}(\mu_K) = g F_1 K_{n+1}(g),$$

or

$$T_K \begin{pmatrix} A_K \\ D_K \end{pmatrix} = F_1 \begin{pmatrix} A_{K+1} \\ D_{K+1} \end{pmatrix}.$$

Then we express coefficient F_1 in terms of A_1 and D_1. Multiple use of relation (3.14) results in

$$T_K \times T_{K-1} \times \ldots \times T_1 \begin{pmatrix} A_1 \\ 0 \end{pmatrix} = T \begin{pmatrix} A_1 \\ 0 \end{pmatrix} = F_1 \begin{pmatrix} K_n(g) \\ g K_{n+1}(g) \end{pmatrix}. \tag{3.15}$$

Numerical solution of eq. (3.15) allows one to find eigenvalues $\hat{\Lambda}$, and the field distribution eigenfunction is obtained by multiple use of relation (3.14).

3.1.4 Gaussian profile

In the case of the gaussian profile of the beam current density (3.1b) there is no beam boundary, so it is natural to perform normalization of the transverse coordinate as $\hat{r} = r/\sqrt{2\sigma_r^2}$. The corresponding reduced variables are as follows:

$$\begin{aligned}
&\hat{z} = \Gamma z, \qquad \hat{\Lambda} = \Lambda/\Gamma, \qquad \hat{C} = C/\Gamma, \\
&\hat{\Lambda}_p^2 = 2c^2(\theta_s\sigma_r\omega)^{-2}, \qquad \hat{\Lambda}_T^2 = \Lambda_T^2/\Gamma^2, \qquad B = 2\Gamma\sigma_r^2\omega/c, \\
&\Lambda_T^2 = < (\Delta\mathcal{E})^2 > \omega^2/(c^2\gamma_z^4\mathcal{E}_0^2) \\
&\Gamma = \left[I\omega^2\theta_s^2/(I_A c^2\gamma_z^2\gamma)\right]^{1/2}, \\
&\hat{D} = i\int_0^\infty \exp\left[-\hat{\Lambda}_T^2\xi^2/2 - \left(\hat{\Lambda} + i\hat{C}\right)\right]\xi d\xi.
\end{aligned} \tag{3.16}$$

In the case of the gaussian beam we use multilayer approximation method (see section 3.1.3) for finding eigenvalues and eigenfunctions.

3.2 Solution of the initial-value problem

To find the evolution of the electric field of the amplified wave $\tilde{E}(z, r, \varphi)$ one should solve the self-consistent field equations under the given conditions at the undulator entrance. In this paper we consider a specific, but practically important case of the following initial conditions:
a) the electron beam is modulated neither in velocity nor density at the undulator entrance;
b) the electric field amplitude $\tilde{E}$ takes the value $\tilde{E}_{ext}(r, \varphi)$ at the undulator entrance.

3.2.1 Stepped profile

In this section we consider the case of axisymmetric electron beam with stepped profile of current density. Introducing the following notations:

$$\begin{aligned}
&\hat{z} = \Gamma z, \qquad \hat{r} = r/r_0, \\
&B = \Gamma r_0^2\omega/c, \qquad \hat{\Lambda}_p^2 = 4c^2/(\omega^2\theta_s^2 r_0^2),
\end{aligned}$$

we write eq. (2.6) in the following reduced form:

Region 1, ($\hat{r} < 1$):

$$\left[\frac{\partial^2}{\partial\hat{r}^2}+\frac{1}{\hat{r}}\frac{\partial}{\partial\hat{r}}+\frac{1}{\hat{r}^2}\frac{\partial^2}{\partial\varphi^2}+2iB\frac{\partial}{\partial\hat{z}}\right]\tilde{E}(\hat{z},\hat{r},\varphi)=$$

$$i\int_0^{\hat{z}}d\hat{z}'\left[2\tilde{E}(\hat{z}',\hat{r},\varphi)+\hat{\Lambda}_{\rm p}^2\left[\frac{\partial^2}{\partial\hat{r}^2}+\frac{1}{\hat{r}}\frac{\partial}{\partial\hat{r}}+\frac{1}{\hat{r}^2}\frac{\partial^2}{\partial\varphi^2}+2iB\frac{\partial}{\partial\hat{z}'}\right]\tilde{E}(\hat{z}',\hat{r},\varphi)\right]\times$$

$$\int_{-\infty}^{\infty}d\xi d\hat{F}(\xi)/d\xi\exp\left[i(\xi+\hat{C})(\hat{z}'-\hat{z})\right], \tag{3.17a}$$

Region 2, $(1<\hat{r})$:

$$\left[\frac{\partial^2}{\partial\hat{r}^2}+\frac{1}{\hat{r}}\frac{\partial}{\partial\hat{r}}+\frac{1}{\hat{r}^2}\frac{\partial^2}{\partial\varphi^2}+2iB\frac{\partial}{\partial\hat{z}}\right]\tilde{E}(\hat{z},\hat{r},\varphi)=0. \tag{3.17b}$$

Then we represent $\tilde{E}$ as a Fourier series in the angle φ:

$$\tilde{E}(\hat{z},\hat{r},\varphi)=\sum_{n=-\infty}^{n=+\infty}\tilde{E}^{(n)}(\hat{z},\hat{r})e^{-in\varphi}.$$

The Laplace transforms of the Fourier coefficients $\tilde{E}^{(n)}$

$$\bar{E}^{(n)}(p,\hat{r})=\int_0^{\infty}e^{-p\hat{z}}\tilde{E}^{(n)}(\hat{z},\hat{r})d\hat{z}$$

are submitted to the following equations:

$$\left[\frac{d^2}{d\hat{r}^2}+\frac{1}{\hat{r}}\frac{d}{d\hat{r}}-\frac{n^2}{\hat{r}^2}+\bar{\mu}^2\right]\bar{E}^{(n)}(p,\hat{r})=\hat{f}^{(n)}(\hat{r}),\qquad \hat{r}<1 \tag{3.18a}$$

$$\left[\frac{d^2}{d\hat{r}^2}+\frac{1}{\hat{r}}\frac{d}{d\hat{r}}-\frac{n^2}{\hat{r}^2}-\bar{g}^2\right]\bar{E}^{(n)}(p,\hat{r})=\hat{f}^{(n)}(\hat{r}),\qquad \hat{r}>1 \tag{3.18b}$$

where notations are introduced:

$$\bar{\mu}^2=-2i\hat{D}\left[1-i\hat{\Lambda}_{\rm p}^2\hat{D}\right]^{-1}-\bar{g}^2,\qquad \bar{g}^2=-2iBp,$$

$$\hat{D}=\int_{-\infty}^{\infty}d\xi\frac{d\hat{F}(\xi)/d\xi}{p+i(\xi+\hat{C})},\qquad \hat{f}^{(n)}(\hat{r})=2iB\tilde{E}^{(n)}_{\rm ext}(\hat{r}).$$

To find $\bar{E}^{(n)}$ one must solve equations (3.18) with the following boundary conditions:

$$\bar{E}^{(n)}(p,\hat{r})\to 0\qquad \text{at } \hat{r}\to\infty,$$

$$\bar{E}^{(n)} \mid_{\hat{r}=1+0} = \bar{E}^{(n)} \mid_{\hat{r}=1-0}, \qquad d\bar{E}^{(n)}/d\hat{r} \mid_{\hat{r}=1+0} = d\bar{E}^{(n)}/d\hat{r} \mid_{\hat{r}=1-0} .$$

Equations (3.18) could be solved using the Green's function method. To find $\tilde{E}^{(n)}(\hat{z},\hat{r})$, the inverse Laplace transformation is used. As a result, in a high-gain limit we obtain [11,13]:

$$\tilde{E}^{(n)} = \sum_{\mathrm{j}} u_{\mathrm{j}} J_n(\mu_{\mathrm{j}}\hat{r}) \exp(\lambda_{\mathrm{j}}\hat{z}), \qquad \hat{r} < 1 \tag{3.19a}$$

$$\tilde{E}^{(n)} = \sum_{\mathrm{j}} u_{\mathrm{j}} \frac{J_{\mathrm{n}}(\mu_{\mathrm{j}})}{K_{\mathrm{n}}(g_{\mathrm{j}})} K_n(g_{\mathrm{j}}\hat{r}) \exp(\lambda_{\mathrm{j}}\hat{z}), \qquad \hat{r} > 1. \tag{3.19b}$$

Here λ_{j} is the jth root of the equation ($\mathrm{Re}(\lambda_{\mathrm{j}}) > 0$):

$$\bar{\mu}(\lambda_{\mathrm{j}}) J_{n+1}\left(\bar{\mu}(\lambda_{\mathrm{j}})\right) K_n\left(\bar{g}(\lambda_{\mathrm{j}})\right) - \bar{g}(\lambda_{\mathrm{j}}) K_{n+1}\left(\bar{g}(\lambda_{\mathrm{j}})\right) J_n\left(\bar{\mu}(\lambda_{\mathrm{j}})\right) = 0$$

where notations have been introduced:

$$u_{\mathrm{j}} = \frac{\left[\frac{K_n(\mu_{\mathrm{j}})}{J_n(g_{\mathrm{j}})}\right] \int_0^1 d\zeta J_n(\mu_{\mathrm{j}}\zeta)\zeta \hat{f}^{(n)}(\zeta) + \int_1^\infty d\zeta K_n(g_{\mathrm{j}}\zeta)\zeta \hat{f}^{(n)}(\zeta)}{\frac{d}{d\lambda}\left[\bar{\mu} J_{n+1}(\bar{\mu}) K_n(\bar{g}) - \bar{g} K_{n+1}(\bar{g}) J_n(\bar{\mu})\right] \mid_{\lambda=\lambda_{\mathrm{j}}}},$$

$$\mu_{\mathrm{j}}^2 = \frac{-2i\hat{D}_{\mathrm{j}}}{1 - i\hat{\Lambda}_{\mathrm{p}}^2 \hat{D}_{\mathrm{j}}} - g_{\mathrm{j}}^2, \qquad g_{\mathrm{j}}^2 = -2iB\lambda_{\mathrm{j}}, \qquad \hat{D}_{\mathrm{j}} = \int_0^\infty d\xi \frac{d\hat{F}(\xi)/d\xi}{\lambda_{\mathrm{j}} + i(\xi + \hat{C})}.$$

Each term in the right-hand sides of expressions (3.19) corresponds to the separate radiation mode and is characterized with the unique amplitude factor, increment and the dependence on the transverse coordinate.

In the paraxial approximation the power gain coefficient G of the radiation mode with the azimuthal index n is given with the expression:

$$G = \int_0^\infty r \mid \tilde{E}^{(n)}(z,r) \mid^2 dr \left[\int_0^\infty r \mid \tilde{E}_{\mathrm{ext}}^{(n)}(r) \mid^2 dr\right]^{-1}.$$

When diffraction parameter B is not very large ($B \lesssim 10$)), one can find that the increment of TEM_{00} mode is visibly greater than the increments of higher TEM_{nk} modes ($n, k = 1, 2, 3, \ldots$) [11,13]. Hence, when the undulator is sufficiently long, the contribution of TEM_{00} mode in expression (3.19) is much more than the contributions of all other modes. In this case we may use the single mode approximation and write:

$$G = 4B^2 \exp(2\,\mathrm{Re}(\lambda_1)\hat{z}) \left| \frac{d}{d\lambda} [\bar{\mu} J_1(\bar{\mu}) K_0(\bar{g}) - \bar{g} K_1(\bar{g}) J_0(\bar{\mu})] \right|_{\lambda=\lambda_1}^{-2} \times$$

$$\left\{ \int_0^\infty \hat{r} \mid \tilde{E}_{\mathrm{ext}}(\hat{r}) \mid^2 d\hat{r} \right\}^{-1} \left\{ \int_0^1 \hat{r} \left| \frac{K_0(g_1) J_0(\mu_1 \hat{r})}{J_0(\mu_1)} \right|^2 d\hat{r} + \int_1^\infty \hat{r} \, |K_0(g_1 \hat{r})|^2 \, d\hat{r} \right\} \times$$

$$\left| \int_0^1 \hat{r} J_0(\mu_1 \hat{r}) \tilde{E}_{\mathrm{ext}}(\hat{r}) d\hat{r} + [J_0(\mu_1)/K_0(g_1)] \int_1^\infty \hat{r} K_0(g_1 \hat{r}) \tilde{E}_{\mathrm{ext}}(\hat{r}) d\hat{r} \right|^2 , \qquad (3.20)$$

where λ_1 is the reduced eigenvalue of TEM_{00} mode.

3.2.2 Arbitrary bounded gradient profile

We have shown above that in the case of the stepped profile of the beam current density, the initial-value problem can be solved analytically using eq. (2.6). When the electron beam has an arbitrary gradient profile of current density (3.1a), one should use the numerical methods to solve the initial problem. The self-consistent field method in the linear approximation enables one to get from the kinetic equation and Maxwell's equations the only equation either for the field amplitude of amplified wave or for the modulation amplitude of the beam current density. Both of the ways lead to the same results but for the analytical calculations it is preferable to use the equation for the wave field (2.6): in this case the mathematical apparatus is always connected with more conventional differential equations. At the same time the situations with the computer simulations is proved to be reversed and the method using the equation for the modulation amplitude of the beam current density (2.8) is more convenient.

In this section we present the algorithm of the initial problem numerical solution using eq. (2.8). The case of axially symmetric radiation field modes is under study. Let us consider the case of negligibly small energy spread. We assume that the field of the master oscillator has the form of the Gaussian laser beam:

$$E_x + iE_y = \tilde{E}_{\mathrm{ext}}(z,r) \exp[i\omega(z/c - t)] = \frac{-iE_g w^2 (\omega/c) e^{-i\omega t}}{2(z - z_0) - iw^2\omega/c} \times$$

$$\exp\left\{ i\frac{\omega}{c}(z - z_0) + \frac{2i(\omega/c)(z - z_0)r^2 - (rw\omega/c)^2}{4(z - z_0)^2 + (w^2\omega/c)^2} \right\} \qquad (3.21)$$

with amplitude

$$E_g = \left[8W_{\mathrm{ext}}/(w^2 c) \right]^{1/2},$$

Here z_0 and w are the position of the focus and the waist size in the focus of the

Gaussian laser beam, respectively and W_{ext} is the total power of the master oscillator. Using standard normalization procedure, we rewrite eq. (2.8) in the form:

$$\frac{d^2\hat{a}_1}{d\hat{z}^2} + 2i\hat{C}\frac{d\hat{a}_1}{d\hat{z}} + \left[\hat{\Lambda}_p^2 - \hat{C}^2\right]\hat{a}_1 = \frac{1}{2i}\hat{U}_r, \tag{3.22}$$

where the following notations are introduced:

$$\hat{a}_1(z,r) = \tilde{j}_1(z,r)\pi r_0^2/I, \qquad \hat{W}_{ext} = W_{ext}/W_0,$$

$$\hat{E}_g = \left[16\hat{W}_{ext}\int_0^1 S(\hat{r})\hat{r}d\hat{r}/(B\hat{w}^2)\right]^{1/2}, \qquad W_0 = I\mathcal{E}_0\Gamma\gamma_z^2 c/(e\omega),$$

$$\hat{U}_r = \hat{U}_{ext}(\hat{z},\hat{r}) + 2i\int_0^{\hat{z}}\frac{d\hat{z}'}{\hat{z}-\hat{z}'}\int_0^1 S(\hat{r}')\hat{r}'d\hat{r}'\hat{a}_1(\hat{z}',\hat{r}')J_0\left(\frac{B\hat{r}\hat{r}'}{\hat{z}-\hat{z}'}\right)\exp\left\{\frac{iB(\hat{r}^2+\hat{r}'^2)}{2(\hat{z}-\hat{z}')}\right\}$$

$$\hat{U}_{ext}(\hat{z},\hat{r}) = -\frac{iB\hat{w}^2\hat{E}_g}{2(\hat{z}-\hat{z}_0)-iBw^2}\exp\left\{\frac{2iB(\hat{z}-\hat{z}_0)\hat{r}^2-(B\hat{w}\hat{r})^2}{4(\hat{z}-\hat{z}_0)^2+(B\hat{w}^2)^2}\right\}. \tag{3.23}$$

Integro-differential equation was solved using computer code FS2RL [11]. Power gain G is calculated with the integration of equation:

$$\frac{dG}{d\hat{z}} = -\frac{1}{\hat{W}_{ext}\int_0^1 S(\hat{r})\hat{r}d\hat{r}}\int_0^1 \hat{r}d\hat{r}\hat{a}_1^*(\hat{r},\hat{z})S(\hat{r})\hat{U}_r + C.C. \tag{3.24}$$

3.2.3 Gaussian profile

In the case of the gaussian profile of the beam current density (3.1b) we normalize the transverse coordinate as $\hat{r} = r/\sqrt{2\sigma_r^2}$. The corresponding reduced variables are given with the expressions (3.16). The only distinction of the equations is that integrals over transverse coordinates in eqs. (3.22), (3.23) and (3.24) are calculated in the limits from 0 to ∞. The function of the beam profile should be taken in the form $S(\hat{r}) = exp(-\hat{r}^2)$.

3.3 Planar undulator

All the results of the linear theory obtained above refer to the case of the helical undulator and circularly polarized radiation. These results can be used also for the case of

a planar undulator and linearly polarized radiation at the following redetermination of the parameters (for the case of the stepped profile):

$$\Gamma = \left[A_{JJ}^2 I\omega^2\theta_1^2(2I_A c^2\gamma_1^2\gamma)^{-1}\right]^{1/2}, \qquad B = r_0^2\Gamma\omega/c,$$

$$C = \kappa_w - \omega/(2c\gamma_1^2), \qquad \hat{\Lambda}_p^2 = 8c^2(\omega^2 r_0^2\theta_1^2 A_{JJ}^2)^{-1},$$

$$\hat{\Lambda}_T^2 = \omega^2 < (\Delta\mathcal{E})^2 > /(c^2\gamma_1^4\Gamma^2\mathcal{E}_0^2), \qquad W_0 = I\mathcal{E}_0\Gamma\gamma_1^2 c/(e\omega).$$

Here we have introduced the following notations:

$$\theta_1 = eH_1/(\mathcal{E}_0\kappa_w), \qquad \gamma_1^{-2} = \gamma^{-2} + \theta_1^2/2.$$

Factor A_{JJ} is given by the formula

$$A_{JJ} = [J_0(\nu) - J_1(\nu)],$$

where $\nu = \theta_1^2\omega/(8c\kappa_w)$, J_0 and J_1 are the Bessel functions.

4 Nonlinear simulations of the FEL amplifier with an axisymmetric electron beam

In the linear mode of the FEL amplifier operation, at sufficiently low input radiation power W_{ext}, an increase of W_{ext} leads to the proportional increase of the output power W_f. When the input power is increased further, the operation of the amplifier becomes to be nonlinear: output power increases more slowly than that input one, and at a certain value of W_{ext} the output power reaches a maximum. To find the FEL characteristics at saturation, it is necessary to solve the equations of the nonlinear theory of the FEL amplifier. The analytical methods are limited in the description of the saturation effects and numerical simulation codes are being used.

The main problems of the nonlinear simulations are connected with the calculation of the radiation and space charge fields. Several different methods are used to calculate the radiation fields: various modifications of the transverse mode spectral method (see e.g. ref. [5]), the finite difference method [6–8] and the Green's function method [12]. In this paper we, following by ref. [12], present an approach to constructing numerical simulation code using Green's function method for the radiation field calculations.

When using the numerical simulation codes the problems are usually arisen of the reliability and the clear physical interpretation of the obtained results. The presented approach satisfies these requirements. First, the model approximations allow one

to check the linear stage of amplification with the rigorous solutions of the linear theory (see section 3). Second, when writing down the final equations we use the similarity techniques. This enables one not only to reduce the number of the problem parameters but also to go over to the variables possessing the clear physical sense. Each physical factor influencing the FEL operation (diffraction, space charge, energy spread etc.) is matched with its own reduced parameter. For the effect under study this reduced parameter is a measure of the corresponding physical effect. When some effect becomes less important for the FEL amplifier operation, this is reflected by the corresponding reduced parameter taking on small values and falling out of the number of the problem parameters.

The presented FEL amplifier model allows one to take into account such effects as the radiation diffraction, space charge fields, energy spread of the electrons in the beam. The initial conditions are considered when one has the radiation from master oscillator (the Gaussian laser beam) and unmodulated electron beam at the undulator entrance. The presented code enables one to calculate the frequency, amplitude and current characteristics of the FEL amplifier. The field distributions in the Fresnel and Fraunhofer zones and various electron beam characteristics could be computed, too. The code allows one to calculate all these characteristics at the constant undulator parameters as well as at the tapering ones.

4.1 Self-consistent equations

To describe motion of electrons in the given electromagnetic field we use canonical equations (2.4). To close the self-consistent problem of the electron beam radiation in the undulator one should find the electromagnetic fields at the given motion of the electrons. Let us write down the Maxwell's wave equations for vector potential $\vec{A}$ and scalar potential ϕ (we use the Lorentz gauge here):

$$\nabla^2\vec{A} - \frac{1}{c^2}\frac{\partial^2}{\partial t^2}\vec{A} = -\frac{4\pi}{c}\vec{j}(\vec{r},t)$$
$$\nabla^2\rho - \frac{1}{c^2}\frac{\partial^2}{\partial t^2}\rho = -4\pi e\rho(\vec{r},t), \qquad (4.1)$$

where $\vec{j}$ is the beam current density and ρ is the beam density. The electric field $\vec{E}$ is connected with potentials $\vec{A}$ and ϕ by relation: $\vec{E} = -c^{-1}\partial\vec{A}/\partial t - \vec{\nabla}\phi$. The solutions of the wave equations (4.1) may be written in the retarded potential form:

$$\vec{A}(\vec{r},t) = \frac{1}{c}\int d\vec{r}' \frac{\vec{j}(\vec{r}', t - |\vec{r}-\vec{r}'|/c)}{|\vec{r}-\vec{r}'|}$$

$$\rho(\vec{r},t) = e\int d\vec{r}'\frac{\rho(\vec{r}',t-\mid\vec{r}-\vec{r}'\mid/c)}{\mid\vec{r}-\vec{r}'\mid}. \tag{4.2}$$

Further we shall consider only the axisymmetric radiation modes. In this case the potentials and the modulation of the beam density do not depend on the azimuthal angle. The integration of equations (4.2) using the paraxial approximation

$$\mid\vec{r}-\vec{r}'\mid\simeq z-z'+\frac{\mid\vec{r}_\perp-\vec{r}'_\perp\mid^2}{2(z-z')}, \tag{4.3}$$

leads to the following expression for the complex amplitude of the radiation field (we keep here only "resonant" part giving nonvanishing contribution in the Hamiltonian after averaging over the undulator period):

$$\tilde{E} = \tilde{E}_{\rm ext} + \frac{2\pi i\omega\theta_{\rm s0}}{c^2}\int\limits_0^z\frac{dz'}{z-z'}\int\limits_0^{r_0} r'dr' j_0(r')\hat{j}_1(z',r')\times \exp\left[\frac{i\omega(r^2+r'^2)}{2c(z-z')}\right]J_0\left(\frac{\omega rr'}{c(z-z')}\right), \tag{4.4}$$

where J_0 is the Bessel function of the first kind, $\tilde{E}_{\rm ext}$ - the complex amplitude of the external radiation field and $\theta_{\rm s0}$ is the rotation angle of the electron with the nominal energy $\mathcal{E}_0$. The reduced complex amplitude of the first harmonic of the beam current density $\hat{j}_1$ is given with the expression:

$$\hat{j}_1 = \frac{<\theta_{\rm k}\exp(-i\psi{\rm k})>}{\theta_{\rm s0}}, \tag{4.5}$$

where symbol $<\ldots>$ means the local averaging over the electrons of the beam, $\theta_{\rm k}$ and $\psi_{\rm k}$ are the rotation angle and the phase of the electron.

For the longitudinal component of the electric field E_z (i.e. for the space charge field) we get the following expression:

$$E_z = \frac{-4\pi i\omega}{\gamma_z^2c^2}\sum_{n=1}^{\infty}ne^{in\psi}\left[K_0\left(\frac{n\omega r}{\gamma_z c}\right)\int\limits_0^r r'dr'\hat{a}_{\rm n}(r',z)j_0(r')I_0\left(\frac{n\omega r'}{\gamma_z c}\right)+ I_0\left(\frac{n\omega r}{\gamma_z c}\right)\int\limits_r^{r_0} r'dr'\hat{a}_{\rm n}(r',z)j_0(r')K_0\left(\frac{n\omega r'}{\gamma_z c}\right)\right]. \tag{4.6}$$

where K_0 and I_0 are the modified Bessel functions and complex amplitudes of the

beam density harmonics $\hat{a}_n$ are given with expression:

$$\hat{a}_n = < \exp(-in\psi_k) > . \tag{4.7}$$

Here, as above, symbol $< \ldots >$ means the local averaging over the electrons of the beam and ψ_k is the phase of the electron. When the transverse electron beam size is rather large (i.e. $r_0^2 \gg \gamma_z^2 c^2/\omega^2$) expression (4.6) for the space charge field E_z takes the form:

$$E_z = -\frac{4\pi i}{\omega} j_0(r) \sum_{n=1}^{\infty} \frac{\hat{a}_n \exp(in\psi)}{n} + C.C. \tag{4.8}$$

Thus, the canonical equations of electron motion (2.4) along with the expressions for electromagnetic field (4.4) and (4.6) describe the self-consistent process of the electron beam radiation amplification in the undulator.

4.2 The reduced working equations

In the same way as it was done in section 3, we use the similarity techniques to write down the working set of equations. When the undulator tapering is performed at the constant undulator parameter K, the system of the canonical equations (2.4) may be rewritten in the following reduced form:

$$\begin{aligned} \frac{d\hat{P}}{d\hat{z}} &= \mathrm{Re}\left[e^{i\psi}\hat{\theta}\hat{U}_r - i\hat{\Lambda}_p^2\hat{U}_c\right] \\ \frac{d\psi}{d\hat{z}} &= \hat{C} + \hat{P}\frac{1+\beta\hat{P}/2}{(1+\beta\hat{P})^2}. \end{aligned} \tag{4.9}$$

Here $\hat{P} = \omega P/(c\gamma_z^2\mathcal{E}_0\Gamma)$, $P = \mathcal{E} - \mathcal{E}_0$, $\beta = c\gamma_z^2\Gamma/\omega$ is the efficiency parameter, $\hat{\theta} = \theta_s/\theta_{s0} = (1+\beta\hat{P})^{-1}$ and all the reduced parameters are given with expressions (3.4). We have neglected small term proportional to $\beta\hat{\theta}\hat{U}_r$ in the right-hand side of the second equation. Normalization procedure is performed using initial parameters of the beam and undulator at the FEL amplifier entrance.

The expression for the effective potential of the radiation field $\hat{U}_r$ entering equations (4.9) is given with expression (3.23).

The reduced complex amplitude of the first harmonic of the beam current density (4.5) $\hat{j}_1 = \mid \hat{j}_1 \mid \cdot \exp(i\psi_1)$ is calculated with the macroparticles ensemble:

$$
\begin{aligned}
\mid \hat{j}_1 \mid &= \frac{1}{N}\left[\left[\sum_{k=1}^{N}\hat{\theta}_{(k)}\cos(\psi_{(k)})\right]^2+\left[\sum_{k=1}^{N}\hat{\theta}_{(k)}\sin(\psi_{(k)})\right]^2\right]^{1/2} \\
\psi_1 &= -\mathrm{arctg}\left[\frac{\sum_{k=1}^{N}\hat{\theta}_{(k)}\sin(\psi_{(k)})}{\sum_{k=1}^{N}\hat{\theta}_{(k)}\cos(\psi_{(k)})}\right]
\end{aligned}
\tag{4.10}
$$

where N is the local number of macroparticles.

The expression for the effective potential of the space charge fields $\hat{U}_c$ is of the form:

$$
\begin{aligned}
\hat{U}_c = \frac{B}{\beta}\sum_{n=1}^{\infty} n e^{in\psi}\Bigg[K_0\left(n\hat{r}\sqrt{B/\beta}\right)\int_0^{\hat{r}} r'd\hat{r}'\hat{a}_{\mathrm{n}}(\hat{r}',\hat{z})I_0\left(n\hat{r}'\sqrt{B/\beta}\right)S(\hat{r}')+ \\
I_0\left(n\hat{r}\sqrt{B/\beta}\right)\int_{\hat{r}}^{1} r'd\hat{r}'\hat{a}_{\mathrm{n}}(\hat{r}',\hat{z})K_0\left(n\hat{r}'\sqrt{B/\beta}\right)S(\hat{r}')\Bigg].
\end{aligned}
\tag{4.11}
$$

When $B/\beta \gg 1$ (which corresponds to the one-dimensional approximation for the space charge field: $r_0^2 \gg \gamma_z^2 c^2/\omega^2$) the expression for U_c takes the following simple form:

$$
\hat{U}_c = S(\hat{r})\sum_{n=1}^{\infty} e^{in\psi}\frac{\hat{a}_{\mathrm{n}}(\hat{r},\hat{z})}{n}.
\tag{4.12}
$$

The beam density modulation harmonics $\hat{a}_n = \mid \hat{a}_n \mid \cdot \exp(i\psi_n)$ are calculated in the same way as in (4.10):

$$
\begin{aligned}
\mid \hat{a}_{\mathrm{n}} \mid &= \frac{1}{N}\left[\left[\sum_{k=1}^{N}\cos(n\psi_{(k)})\right]^2+\left[\sum_{k=1}^{N}\sin(n\psi_{(k)})\right]^2\right]^{1/2} \\
\psi_{\mathrm{n}} &= -\mathrm{arctg}\left[\frac{\sum_{k=1}^{N}\sin(n\psi_{(k)})}{\sum_{k=1}^{N}\cos(n\psi_{(k)})}\right].
\end{aligned}
$$

The power gain coefficient G is calculated with the integration of the equation (3.24).

The field distribution in the Fresnel diffraction zone (i.e. inside the undulator) is given with expressions (3.23) and (??). At the large distance of z from the undulator exit, the radiation has the form of a spherical wave with the amplitude depending on an observation angle $\theta = r/z$. The directivity diagram of the radiation intensity is proportional to the square of the field amplitude:

$$\Xi(\hat{\theta}) = \int_0^{\hat{l}_w} d\hat{z} \int_0^1 d\hat{r}\hat{r}\hat{j}_1(\hat{z},\hat{r})S(\hat{r})\exp\left(i\hat{\theta}^2\hat{z}/B\right)J_0(\hat{\theta}\hat{r}) -$$
$$i\frac{\hat{E}_g\hat{w}^2B}{4}\exp\left[-\frac{i\hat{\theta}^2\hat{z}_0}{2B} - \frac{\hat{w}^2\hat{\theta}^2}{4}\right],$$

where $\hat{l}_0 = \Gamma_0 l_0$ is the reduced undulator length and $\hat{\theta} = r_0\omega\theta/c$ is the reduced observation angle.

It should be emphasized that the system of working equations (4.9) has been derived using Hamiltonian (2.3) and we have not done severe restrictions on the electron energy deviation from the initial value: we have only omitted the members with the order of $1/\gamma^2$ in the right-hand sides of equations (4.9). Hence, system (4.9) allows one to simulate the FEL amplifiers with high efficiency η up to the unit (of course, the final electron energy must be sufficiently large, i.e. $\gamma_f \gg 1$).

4.2.1 Gaussian profile

In the case of the gaussian profile of the beam current density (3.1b) we normalize the transverse coordinate as $\hat{r} = r/\sqrt{2\sigma_r^2}$. The corresponding reduced variables are given with the expressions (3.16). The only distinction of the equations is that integrals over transverse coordinates in eqs. (??) and (4.11) are calculated in the limits from 0 to ∞. The function of the beam profile should be taken in the form $S(\hat{r}) = exp(-\hat{r}^2)$.

4.3 Simulation code FS2RN

We have realized the above described algorithm in the computer code FS2RN. The simulation is performed with the macroparticle method. The macroparticle ensemble is prepared as follows: the electron beam is divided into M layers over the radius and in each layer we distribute uniformly N macroparticles over phase ψ from 0 to 2π. The initial energy spread is simulated with the additional distribution of the particles according to the Gaussian law:

$$dw = \frac{1}{\sqrt{2\pi\hat{\Lambda}_T^2}}\exp\left[-\frac{\hat{P}^2}{2\hat{\Lambda}_T^2}\right]d\hat{P},$$

where $\hat{\Lambda}_T^2 = \Lambda_T^2/\Gamma^2 =< (\Delta\mathcal{E})^2 > \omega^2/(c^2\gamma_z^4\mathcal{E}_0^2\Gamma^2)$ is the energy spread parameter.

As a result we get the system of $2 \times N \times M$ ordinary differential equations (4.9) which is integrated with the Runge-Kutta scheme. It should be noted that the standard

numerical quadratures are not effective for the calculation of the integral over z' in expression (??) as the integrand has an singularity at $z' \to z$. To calculate this integral we have developed a special algorithm. The integration interval $(0, z)$ is divided into some number of subintervals and $\hat{j}_1$ is approximated with the polynomials in each of them. The Bessel function $J_0(t)$, where $t = B\hat{r}\hat{r}'/(\hat{z} - \hat{z}')$, is approximated with the polynomials at small values of t and at large values of t we use the asymptotic expansion. As a result the calculation of integral (??) over z' is reduced to the sum of special functions: Fresnel integrals, integral sine and cosine. The definite integral over the transverse coordinate in expression (??) is calculated with the standard quadrature formulae.

We have carefully tested code FS2RN in two different ways:

i) at the linear stage of operation - with the programs of FS2R package: FS2RD (the analysis of the eigenvalue problem) and FS2RL (the initial-value problem solution) [11,13];

ii) at the nonlinear stage - with the programs of WG2R package developed for the calculation of the FEL amplifier with a circular waveguide (the testing has been performed in the asymptote of the large waveguide radius) [18].

4.4 Applicability region

The basic peculiarities of our approach are the three-dimensional representation of the radiation and space charge fields, and the electron motion description with the one-dimensional approximation. This model, to some extent, tends to simplify real processes occurring in the FEL amplifiers. However, within the scope of such a model we take into account almost all the main effects influencing the FEL amplifier operation: diffraction of radiation, space charge fields and energy spread of electrons in the beam. It should be noted that in the framework of the presented model the beam emittance influence on the FEL amplifier operation has been fallen out of the consideration. To be strict, this effect should be taken into account in the framework of the fully three-dimensional theory and the results, obtained with this model, should be considered as a reliable test basis for the more complicated models. As for upgrading the numerical simulation algorithm, it is not a physical problem but computational one and can be easily resolved. Situation with upgrading the linear theory is much more complicated and there is no possibility to obtain rigorous analytical results (see, e.g. ref. [9]).

When deriving self-consistent equation (2.6) of the linear mode of operation and constructing the numerical simulation algorithm we have neglected betatron oscillations of the particles. On the other hand, when moving in the undulator field, particles

perform betatron oscillations. The wavelength of betatron oscillations is

$$\lambda_b = 2^{1/2}\lambda_w\theta_s^{-1}. \tag{4.13}$$

So, the reasonable question is arisen when this model describes correctly the real processes in the FEL amplifier. Simple physical considerations show that it takes place in two cases. First, this model is valid when the betatron oscillation wavelength is much more than characteristic length of the radiation field growth. In the linear mode of operation this length is of the order of the gain length. Second situation corresponds to such a choice of the FEL amplifier parameters which provide the characteristic transverse size of the radiation field eigenmode to be much more than the transverse size of the electron beam. In this cases the emittance effects can be taken into account as follows. As a rule, the electron beam should be matched with the focusing system of the undulator which results in the following values of the beam radius r_0 and angle spread $(<(\Delta\theta)^2>)^{1/2}$ of the electrons in the beam:

$$r_0 = (\beta_w\epsilon_n/\gamma\pi)^{1/2}, \qquad (<(\Delta\theta)^2>)^{1/2} = (\epsilon_n/\pi\beta_w\gamma)^{1/2} \tag{4.14}$$

where $\beta_w = \sqrt{2}\,\lambda_w/2\pi\theta_w$ is the beta-function of the electron beam in the undulator and ϵ_n is the normalized emittance of the beam. The presence of the angle spread in the beam results in additional spread in the longitudinal velocities which may be interpreted with introducing of additional energy spread. So, the inclusion of the emittance effects is performed by substituting the real energy spread $\sigma_E = [<(\Delta\mathcal{E}/\mathcal{E})^2>]^{1/2}$ in the energy spread parameter

$$\hat{\Lambda}_T^2 = \sigma_E^2\omega^2/(c^2\gamma_z^4\mathcal{E}_0^2\Gamma^2)$$

by "effective" energy spread

$$\sigma_E = [<(\Delta\mathcal{E}/\mathcal{E})^2> + \gamma_z^4 <(\Delta\theta)^2>^2 /4]^{1/2}.$$

Another limitation of the model is that the radius of the electron rotation r_w in the undulator must be much less than the radius of electron beam r_0 which results in the following limitation on the electron beam emittance:

$$r_w^2 = (\theta_w\lambda_w/2\pi)^2 \ll \epsilon_n\lambda_b/2\pi\gamma. \tag{4.15}$$

One more approximation of the model refers to the linear mode of the FEL amplifier operation. When deriving eq. (2.6) we have neglected the reduction of the plasma frequency due to finite transverse size of electron beam. This condition assumes the transverse electron beam size to be rather large, $r_0^2 \gg \gamma_z^2c^2/\omega^2$ which corresponds to the following limitation on the emittance value:

$$(\gamma_{z0}\lambda/2\pi)^2 \ll \epsilon_n\lambda_b/2\pi\gamma. \tag{4.16}$$

It is interesting to notice that conditions (4.15) and (4.16) are almost identical at a large value of the undulator parameter $K = eH_w\lambda_w/2\pi mc^2$.

When the FEL amplifier parameters satisfy the above mentioned conditions, the presented model provide reliable results when the emittance effects are taken into account in the way described above.

5 Shot noise in the FEL amplifier

Let us present simple derivation of the "effective" power of noise at the FEL amplifier entrance. We assume that the number of electrons emitting from the cathode fluctuates randomly in time near the mean value I. First, we remember that the length of longitudinal coherence (or cooperation length) is:

$$l_c \simeq \lambda l_g/\lambda_w, \tag{5.1}$$

where $l_g \simeq 1/\Gamma$ is the gain length.

First we consider the case of thin electron beam. In this case the expansion of radiation at the gain length is much more than transverse size of the electron beam, $\lambda l_g \gg S_b$, and the number of electrons in the volume of coherence is

$$N \simeq Il_c/ec, \tag{5.2}$$

and amplitude of modulation of the beam current is

$$\hat{a} \simeq 1/\sqrt{N} = 1/\sqrt{Il_c/ec}. \tag{5.3}$$

To calculate the radiation power at the gain length produced by such initial modulation of the beam current, we should remember that the power of coherent radiation is proportional to the square of the beam modulation and that the power generated by totally bunched beam ($\hat{a} \simeq 1$) at the gain length is equal to:

$$W_{sat} \simeq \beta\mathcal{E}_0 I/e, \tag{5.4}$$

where $\beta = \Gamma/\kappa_w$ is saturation parameter and $\Gamma = [I\omega^2\theta_s^2/(I_A c^2\gamma_z^2\gamma)]^{1/2}$. Taking into account eq. (5.3) and omitting numerical coefficient, we find that the radiation power at the gain length produced by shot noise of the beam current is equal to:

$$W_{sh} \simeq eI\omega\gamma_z^2\theta_s^2/c. \tag{5.5}$$

So, in the case of thin electron beam the "effective" power of shot noise at the FEL amplifier entrance depends on the total beam current and not on the beam transverse dimensions.

Situation with the wide electron beam is much more complicated. In this case expansion of radiation at the gain length is much less than transverse size of the electron beam, $\lambda l_g \ll S_b$. First, we see that there is no total transverse coherence of the shot noise at the entrance of the undulator. Using simple physical assumptions, we can suppose that in the initial stage the process of the amplification develops independently inside clusters with transverse square:

$$S_{cl} \sim \left[\frac{I_A \gamma_z^2 \gamma c^4}{j_0 \omega^4 \theta_s^2}\right]^{1/3}, \tag{5.6}$$

where $j_0 = I/S_b$. Total current in each cluster is $I_{cl} \sim IS_{cl}/S_b$. Using the same considerations, as it was presented above, and omitting numerical coefficient, we obtain the value of the "effective" power of input signal in the cluster:

$$W_{sh} \simeq eI_{cl}\omega\gamma_z^2\theta_s^2/c, \tag{5.7}$$

In conclusion we should note that simple qualitative considerations give reliable estimation (5.5) for mean "effective" power of the shot noise in the case of thin electron beam. In the case of wide electron beam situation is much more complicated. We can suppose only that the process of amplification from shot noise develops independently in clusters and can only estimate "effective" power of shot noise in the cluster. As for the further development of the process, we can suppose that there could be a situation when some cluster begin to swallow up his neighbors. As a result, the square of transverse coherence will be increased and finally it could occupy all cross-section of the beam. Nevertheless, simple qualitative consideration can not describe this process and three-dimensional numerical simulations should be performed in the same way as it was done in one-dimensional model (see ref. [19] and references therein).

6 Calculations of the SASE FEL

In this section we present the results of calculations with FS2R program package of the SASE FEL characteristics. General parameters of the 6 nm and 70 nm options of the SASE FEL are presented in Table 1. We assume the transverse phase space distribution of the particles in the beam to be gaussian and the beam is matched with the magnetic system of the undulator. The beam current density is given by eq. (3.1b) and the rms beam size and rms angle spread of the electrons in the beam are

given by the expressions:

$$\sigma_r = \sqrt{\epsilon_n \beta_f / \gamma}, \qquad \sigma_\theta = \sqrt{\epsilon_n / \beta_f \gamma},$$

where β_f is beta-function and ϵ_n is the rms normalized emittance.

We assume the energy spread to be the gaussian:

$$dw = \frac{\exp(-\mathcal{E}^2/2\sigma_E^2)}{\sqrt{2\pi\sigma_E^2}} d\mathcal{E}.$$

When effects of the space charge field and energy spread are negligible:

$$\begin{aligned} &4I/(\gamma I_A \beta B^{1/3}) \ll 1, \qquad &&< (\Delta\mathcal{E}/\mathcal{E})^2 > /(\beta^2 B^{-2/3}) \ll 1, \qquad &&\text{at } B \geq 1, \\ &4I/(\gamma I_A \beta B) \ll 1, \qquad &&< (\Delta\mathcal{E}/\mathcal{E})^2 > /\beta^2 \ll 1, \qquad &&\text{at } B \lesssim 1, \end{aligned} \tag{6.1}$$

the main characteristics of the FEL amplifier could be expressed in terms of the gain parameter Γ, diffraction parameter B and saturation parameter β [11,12]:

Maximal value of the increment:

$$\mathrm{Re}(\Lambda) \simeq \begin{cases} \Gamma B^{-1/3} & \text{at } B \geq 1 \\ \Gamma & \text{at } B \lesssim 1, \end{cases} \tag{6.2}$$

Efficiency at the saturation $\eta_{sat} = P_{sat}/P_{beam}$:

$$\eta_{sat} \simeq \begin{cases} \beta B^{-1/3} & \text{at } B \geq 1 \\ \beta & \text{at } B \lesssim 1. \end{cases} \tag{6.3}$$

So, we see that to obtain maximal efficiency and shorter undulator length, it is necessary to focus the electron beam to provide the value of the diffraction parameter $B \sim 1$. At decreasing the size of the electron beam, the requirements on the value of the energy spread become to be less severe:

$$\frac{\Delta\mathcal{E}}{\mathcal{E}} \lesssim \begin{cases} 0.5\beta B^{-1/3} & \text{at } B \geq 1 \\ 0.5\beta & \text{at } B \lesssim 1, \end{cases} \tag{6.4}$$

while the requirements on the value of the emittance become to be more severe:

$$\epsilon \lesssim \begin{cases} 0.5\lambda B^{1/3} & \text{at } B \geq 1 \\ 0.5\lambda B^{1/2} & \text{at } B \lesssim 1 \end{cases} \tag{6.5}$$

Due to technical reasons the values of the external beta-function have been chosen to be $\beta_f = 300$ cm and $\beta_f = 90$ cm for 6 nm and 70 nm options, respectively [20]. At chosen value of the external focusing the value of the space charge parameter for the both cases is significantly less than 0.1, so the influence of the space charge fields on the process of the field amplification is negligible. Nevertheless, we see from Table 1 that in the both cases the value of the energy spread parameter $\hat{\Lambda}_T^2$ is rather large and there is no significant safety margin with respect to the energy spread of the electrons in the beam.

In calculations we have simulated initial conditions for the input signal as gaussian laser beam. The value of "effective" power of the input signal due to fluctuations of the beam current density has been chosen in accordance with (5.5):

$$W_{sh} \simeq eI\gamma_z^2\theta_s^2\omega/c$$

6.1 Influence of the emittance

Figs.1-4 allow one to trace the influence of the emittance on the operation of the FEL amplifier. We see that for the both cases the project value of the emittance is within the safe bounds. Even a significant increase of the emittance could not destroy the FEL operation. Decrease of the FEL output power with the emittance increase is defined mainly with diffraction effects. The corresponding increase of the longitudinal velocity spread gives a small contribution to the efficiency decrease.

6.2 Influence of the energy spread

In Figs.5-8 we illustrate the influence of the energy spread of the particles in the beam on the FEL amplifier operation. Analysis of these plots indicates that there is no significant safety margin for the energy spread. In the both cases, an increase of the energy spread by a factor of 3 almost destroy the FEL amplifier operation.

6.3 Influence of the beam current deviation

The plots presented in Figs.1-8 have been calculated at the nominal values of the peak beam current. The plots presented in Fig.9 allow one to formulate the requirements on the beam current deviation from the nominal value.

6.4 Output characteristics

The plots in Figs.2 and 5 present the dependencies of the peak output power versus the undulator length. The plots in Fig.10 present axial distribution of the peak radiation power and the plots in Fig.11 – the average output power versus the length of the undulator.

In Fig.12 we present the frequency characteristics of the FEL amplifier. Remembering that the input signal has appearance of the "white" noise, we can conclude that in the both cases the spectral width of the SASE FEL will be $\Delta\lambda/\lambda \sim 0.5$ %.

The plots in Fig.13 present the transverse field distribution inside the undulator and Fig.14 presents the directivity diagrams of the radiation in the Fraunhofer diffraction zone.

As the input signal has appearance of the shot noise, its amplitude fluctuates near average value according to Poisson statistics. Thus, a reasonable question arises about fluctuations of the output power. Analysing plots, presented in Fig.15, we can conclude that there is very simple method to suppress the influence of the fluctuations of the input signal on the output power. First, we calculate the saturation length of the undulator at the nominal value of the input signal. Then we choose the undulator length to be approximately by two e-fold lengths greater than this value. As a result, we obtain that in the wide region of the fluctuations of the input power (four orders of magnitude) the fluctuations of the output power are of about 20 %.

7 Discussion

In conclusion we should like to discuss the validity of performed calculations. First, we did not mentioned the problem of transverse and longitudinal coherence of the output radiation of the SASE FEL. Strictly speaking, the steady-state approximation can not provide quantitative description of this phenomenon. Nevertheless, we can perform some simple physical estimations. As for the length of the longitudinal coherence, it is of the order of cooperation length: $l_c \simeq \lambda l_g/\lambda_w$, where $l_g \simeq 1/\Gamma$ is the gain length. So, if the length of the electron beam σ_z is significantly greater than the cooperation length, there will be temporal dependence of the frequency and amplitude of the

output radiation within each pulse. The number of spikes in each pulse is of the order of σ_z/l_c. While the fluctuations of the amplitude of these spikes could be done rather small, the wavelength will fluctuate from one spike to another one within the bandwidth given by the plots in Fig.12. The results obtained in the framework of the one-dimensional model confirm these simple physical considerations [19].

Situation with the transverse coherence of the output signal is somewhat complicated. We have mentioned in section 5 that in the case of the small diffraction parameter ($B \lesssim 1$), there is total transverse coherence of the input signal from the very beginning of undulator. As a result, we will obtain total transverse coherence of the output signal. The case of the 70 nm option of the SASE FEL meets this condition, so we can conclude that all the results of calculations in the framework of steady-state model could be applicable to the case of the SASE FEL.

In the case of 6 nm option, the value of the diffraction parameter is $B \sim 10$ and there is no total transverse coherence of the input signal at the amplifier entrance. With respect to this, the calculations of the 6 nm option could be referred to the SASE FEL very carefully. All the calculations have been performed for the input radiation with the total transverse coherence. In the real situation the input conditions are quite different. The process of amplification develops from several clusters with different frequencies and amplitudes. Even in the case when some cluster will swallow up all his neighbors, we can not estimate carefully the length at which this competition process takes place. As a result, there could be an error in estimation of the required length of the undulator. As for another output characteristics of the radiation (frequency bandwidth, field distribution, the value of the output radiation power), they are predicted rather carefully by the steady-state calculation if there is settled total transverse coherence in the end of the undulator.

Finally, we can conclude that the steady-state model provides a firm base for calculations of the SASE FEL in the case of the small diffraction parameter and calculation of the 70 nm option of the SASE FEL could be performed in this way. As for the case of 6 nm option, a three-dimensional time-dependent code should be developed to obtain more correct results.

Acknowledgement

We express deep gratitude to our colleagues at DESY due to which hospitality and support it became possible to perform this investigation. We are extremely grateful to W. Brefeld, B. Faatz, R. Rossbach, J. Pflueger and P. Pierini for many useful discussion and fruitful cooperation. We thank B.H. Wiik, D. Trines and I. Ivanov for their interest in our work.

References

[1] C. Pellegrini et al., Nucl. Instrum. and Methods **A341**(1994)326

[2] H. Edwards, editor, "TESLA Test Facility Linac: Conceptual Design Report", Hamburg, DESY, December 5, 1994.

[3] G.T. Moore, Opt. Commun. **52**(1984)46

[4] G.T. Moore, Nucl. Instrum. and Methods **A250**(1986)381

[5] C.-M. Tang and P. Sprangle, IEEE J. Quantum Electron. **QE-21**(1985)970

[6] E.T. Scharlemann and W.M. Fawley, Proc. SPIE 642 (1986)2

[7] T.M. Tran and J.S. Wurtele, Comput. Phys. Commun. **54**(1989)263

[8] J.C. Goldstein, T.F. Wang, B.E. Newnam, and B.D. McVey, Proc. 1987 Particle Accelerators Conf., Washington, DC, USA, p.202

[9] L.H. Yu, S. Krinsky and R.L. Glukstern, Nucl. Instrum. and Methods **A304**(1991)516

[10] Y.H. Chin, K.-J. Kim and M. Xie, Nucl. Instrum. and Methods **A318**(1992)481

[11] E.L. Saldin, E.A. Schneidmiller and M.V. Yurkov, Opt. Commun. **97**(1993)272

[12] E.L. Saldin, E.A. Schneidmiller and M.V. Yurkov, Opt. Commun. **95**(1993)141

[13] E.L. Saldin, E.A. Schneidmiller and M.V. Yurkov, Preprint DESY 94-219, Hamburg, DESY, 1994.

[14] M. Born and E. Wolf, Principles of optics (Pergamon Press, London, 1959)

[15] M.I. Adams, An introduction to optical waveguides (Wiley, New York, 1981)

[16] E.L. Saldin, E.A. Schneidmiller and M.V. Yurkov, Opt. Commun. **87**(1992)69

[17] E.L. Saldin, E.A. Schneidmiller and M.V. Yurkov, Nucl. Instrum. and Methods **A317**(1992)581

[18] E.L. Saldin, E.A. Schneidmiller and M.V. Yurkov, Sov. Voprosy Atomnoi Nauki i Tekhniki (Seria Yaderno-Phys. Issl.) 6(1990)90, in Russian.

[19] R. Bonifacio et al., Nucl. Instrum. and Methods **A341**(1994)181

[20] "A VUV Free Electron Laser at the TESLA Test Facility at DESY. Conceptual Design Report", DESY, Hamburg, April, 1995

Table 1
General parameters of 6 nm and 70 nm SASE FEL

	6 nm option	70 nm option
Electron beam		
Energy, $\mathcal{E}$	1000 MeV	300 MeV
Peak current, I	2500 A	600 A
Normalized rms emittance (Gaussian), ϵ_n	10^{-4} cm rad	2×10^{-4} cm rad
rms energy spread (Gaussian), $\sigma_E/\mathcal{E}$	0.1 %	0.17 %
rms bunch length, σ_z	5×10^{-3} cm	2×10^{-2} cm
Bunch separation	125 ns	125 ns
Number of bunches per train	6400	6400
Repetition rate	10 Hz	10 Hz
External β-function, β_f	300 cm	90 cm
rms beam size in the undulator, σ_r	4×10^{-3} cm	5.5×10^{-3} cm
Undulator		
Type	Planar	Planar
Period, λ_w	2.73 cm	2.73 cm
Peak magnetic field, H_w	4.972 kGs	4.972 kGs
Undulator parameter, K	0.896	0.896
Radiation		
Wavelength, λ	6.421 nm	71.2 nm
Effective power of shot noise	1 kW	50 W
Reduced parameters		
Gain parameter, Γ	2.33×10^{-2} cm^{-1}	2.09×10^{-2} cm^{-1}
Diffraction parameter, B	7	1.13
Space charge parameter, $\hat{\Lambda}_p^2$	8.6×10^{-3}	4.7×10^{-2}
Energy spread parameter $\hat{\Lambda}_T^2$	0.11	0.14
Saturation parameter, β	0.005	0.0045

(a) 6 nm option. Here $\sigma_E/\mathcal{E} = 0.1$ %.

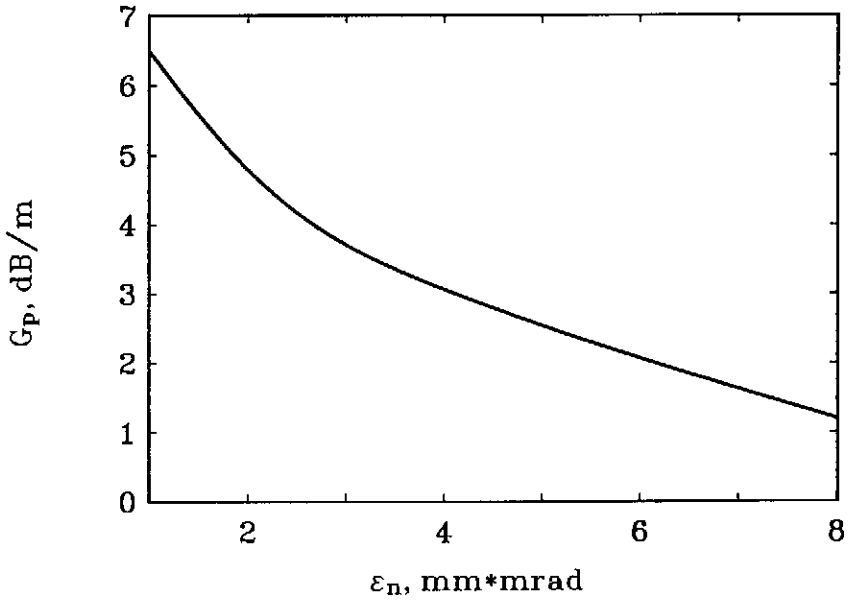

(b) 70 nm option. Here $\sigma_E/\mathcal{E} = 0.17$ %.

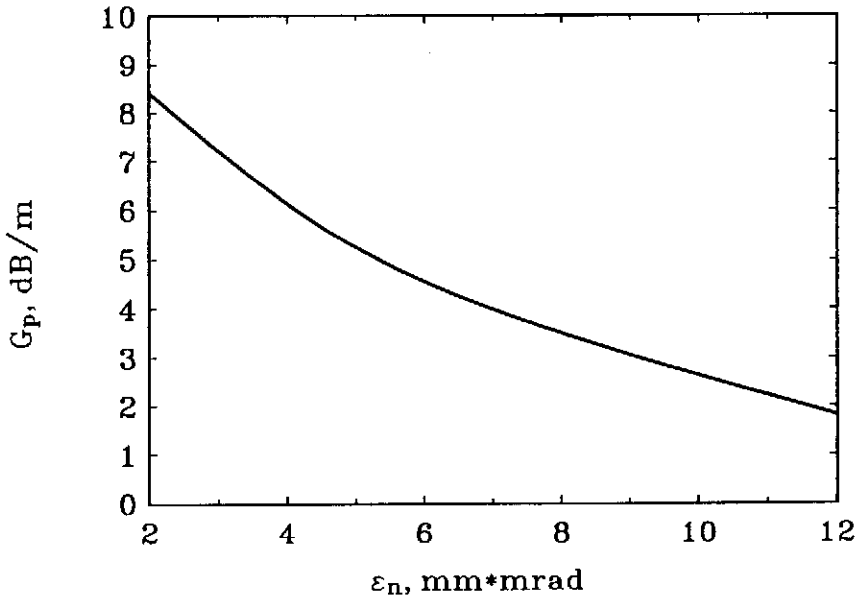

Fig. 1. Dependence of the maximal power gain in the high-gain limit on the value of the normalized emittance.

(a) 6 nm option. (1): $\epsilon_n = 10^{-4}$ cm rad, (2): $\epsilon_n = 2 \times 10^{-4}$ cm rad, (3): $\epsilon_n = 4 \times 10^{-4}$ cm rad. Here $\sigma_E/\mathcal{E} = 0.1$ %.

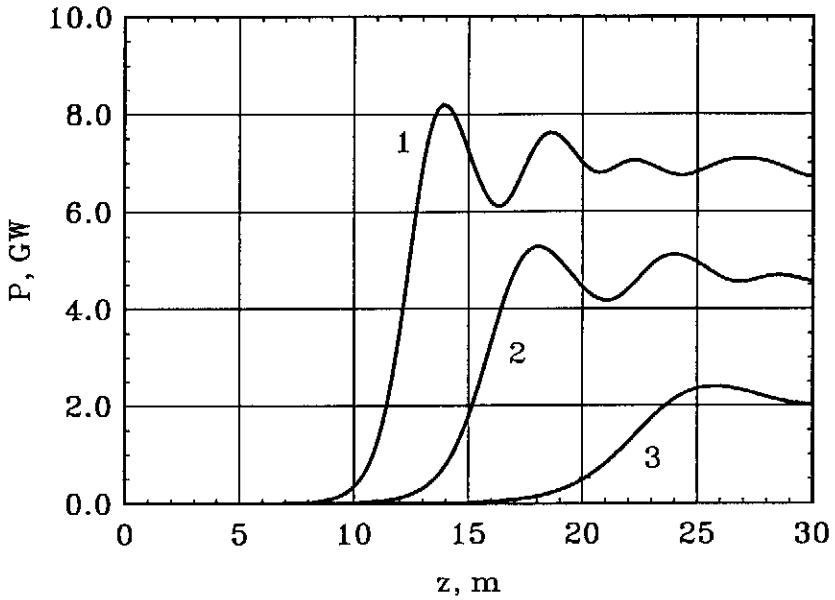

(b) 70 nm option. (1): $\epsilon_n = 2 \times 10^{-4}$ cm rad, (2): $\epsilon_n = 4 \times 10^{-4}$ cm rad, (3): $\epsilon_n = 8 \times 10^{-4}$ cm rad. Here $\sigma_E/\mathcal{E} = 0.17$ %.

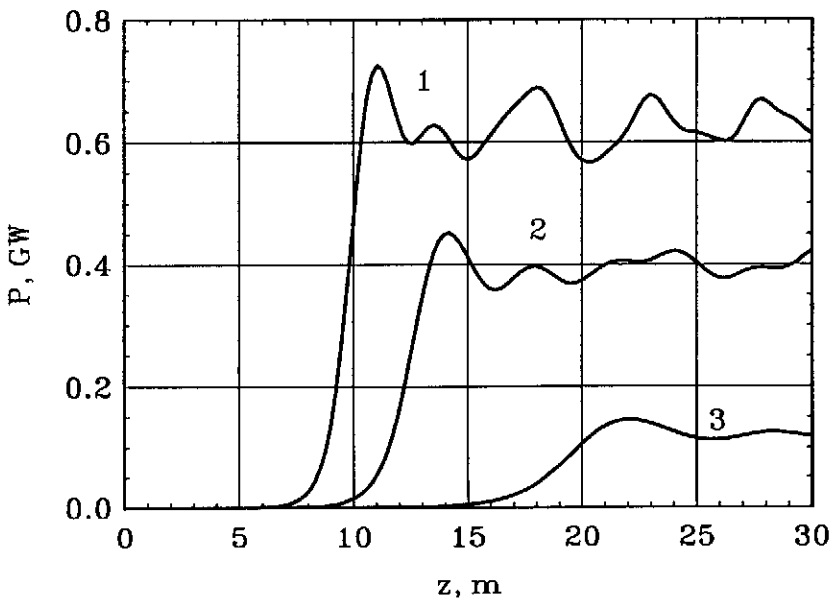

Fig. 2. Dependence of the output power on the undulator length.

(a) 6 nm option. Here $\sigma_E/\mathcal{E} = 0.1$ %.

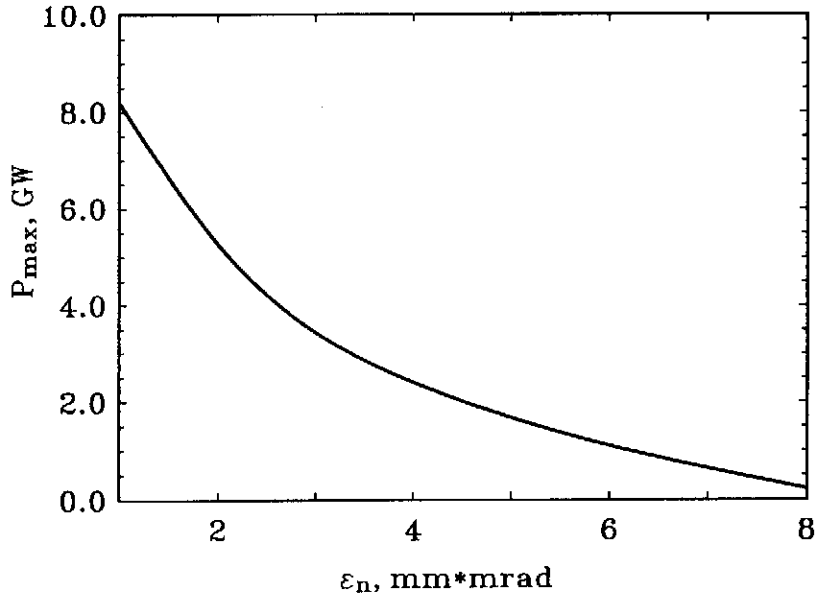

(b) 70 nm option. Here $\sigma_E/\mathcal{E} = 0.17$ %.

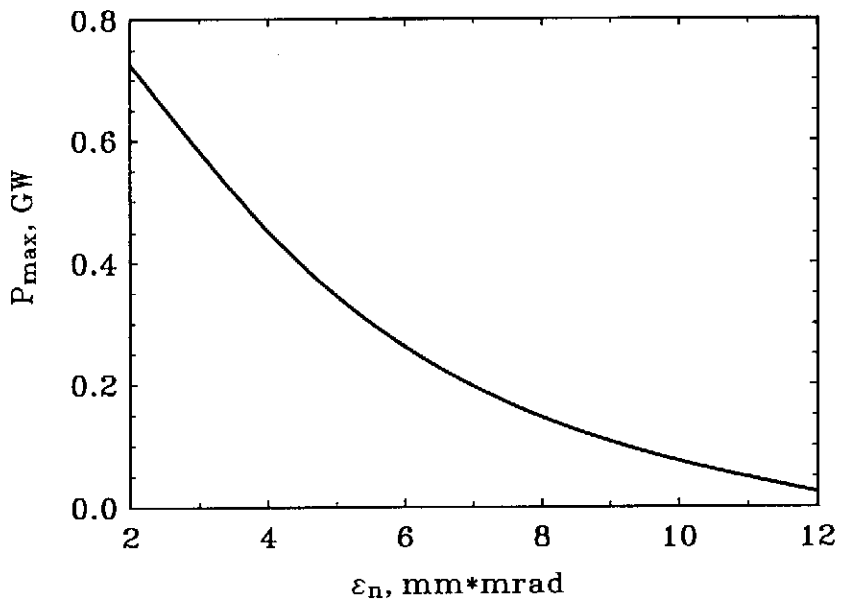

Fig. 3. Dependence of the maximal output power on the value of the normalized emittance.

(a) 6 nm option. Here $\sigma_E/\mathcal{E} = 0.1$ %.

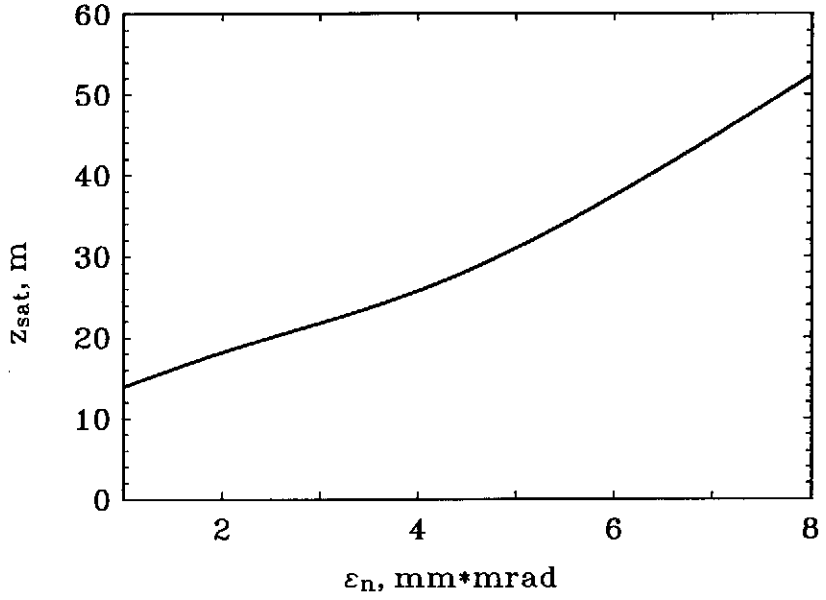

(b) 70 nm option. Here $\sigma_E/\mathcal{E} = 0.17$ %.

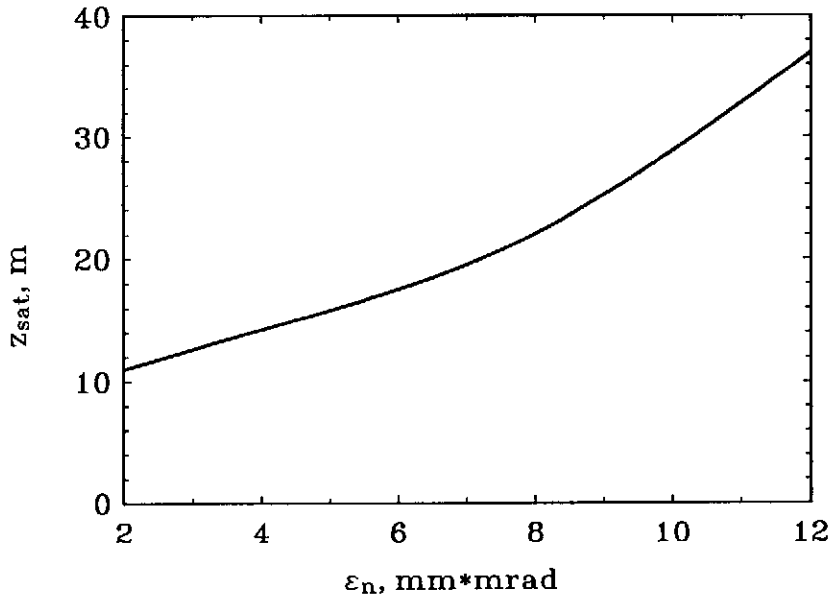

Fig. 4. Saturation length versus emittance.

(a) 6 nm option. Here $\epsilon_n = 10^{-4}$ cm rad.

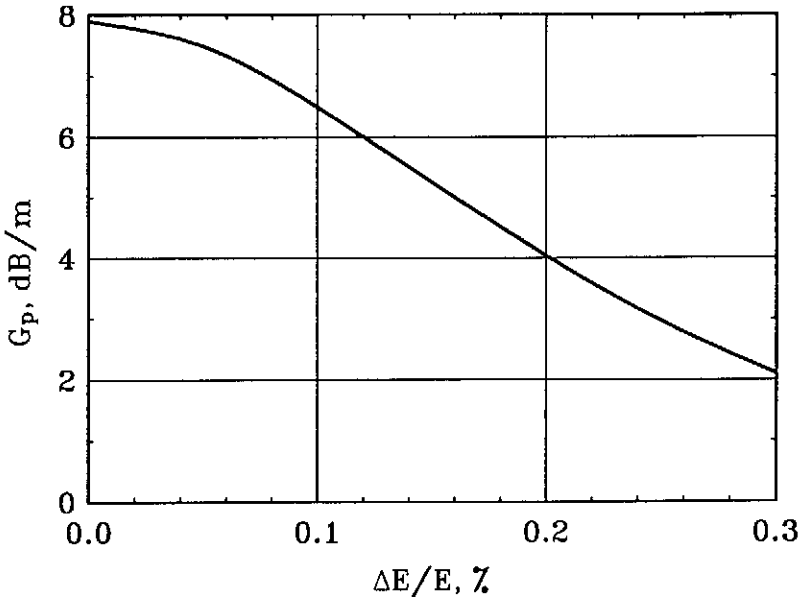

(b) 70 nm option. Here $\epsilon_n = 2 \times 10^{-4}$ cm rad.

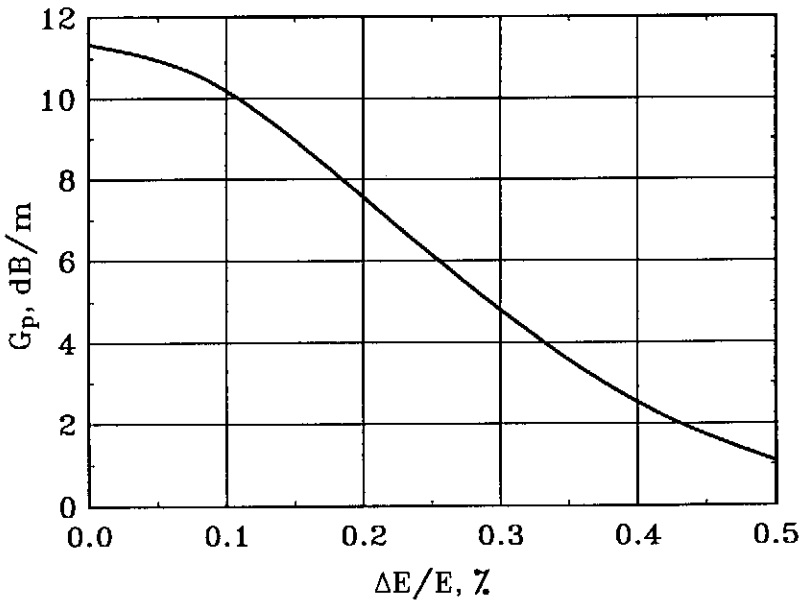

Fig. 5. Dependence of the maximal power gain in the high-gain limit on the value of the energy spread.

(a) 6 nm option. (1): $\sigma_E/\mathcal{E} = 0.1$ %, (2): $\sigma_E/\mathcal{E} = 0.2$ %, (3): $\sigma_E/\mathcal{E} = 0.3$ %. Here $\epsilon_n = 10^{-4}$ cm rad.

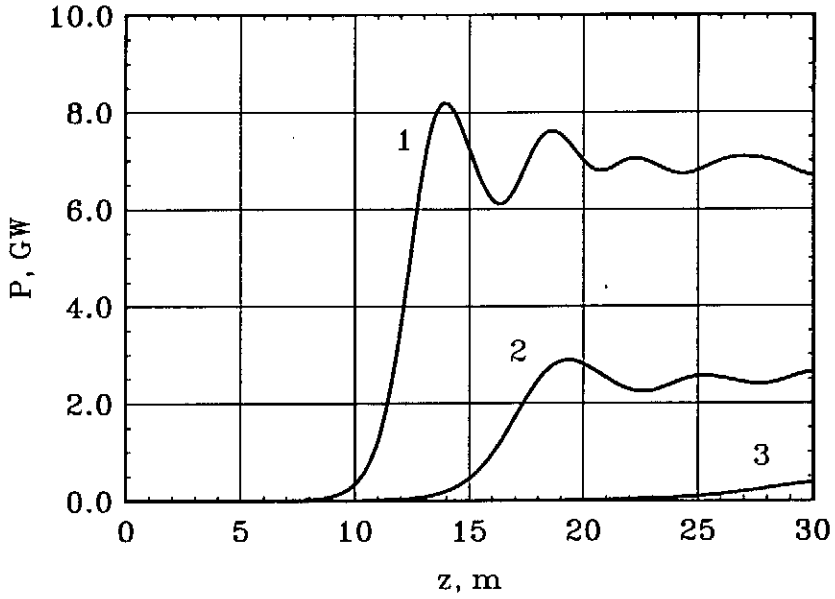

(b) 70 nm option. (1): $\sigma_E/\mathcal{E} = 0.17$ %, (2): $\sigma_E/\mathcal{E} = 0.25$ %, (3): $\sigma_E/\mathcal{E} = 0.35$ %. Here $\epsilon_n = 2 \times 10^{-4}$ cm rad.

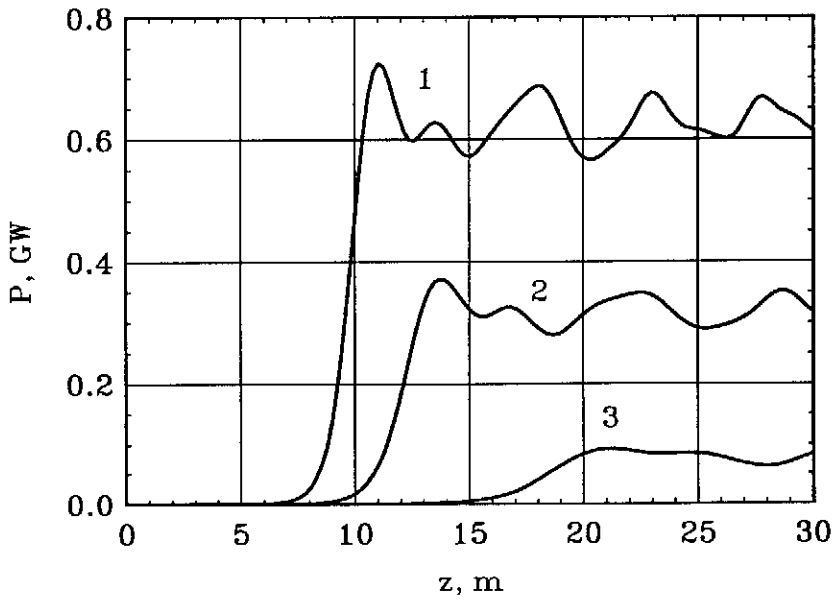

Fig. 6. Dependence of the output power on the undulator length.

(a) 6 nm option. Here $\epsilon_n = 10^{-4}$ cm rad.

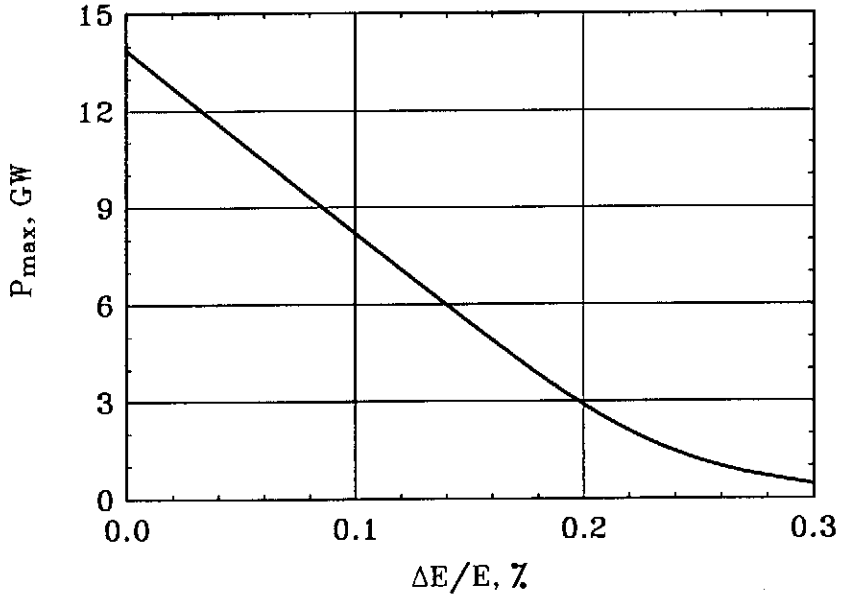

(b) 70 nm option. Here $\epsilon_n = 2 \times 10^{-4}$ cm rad.

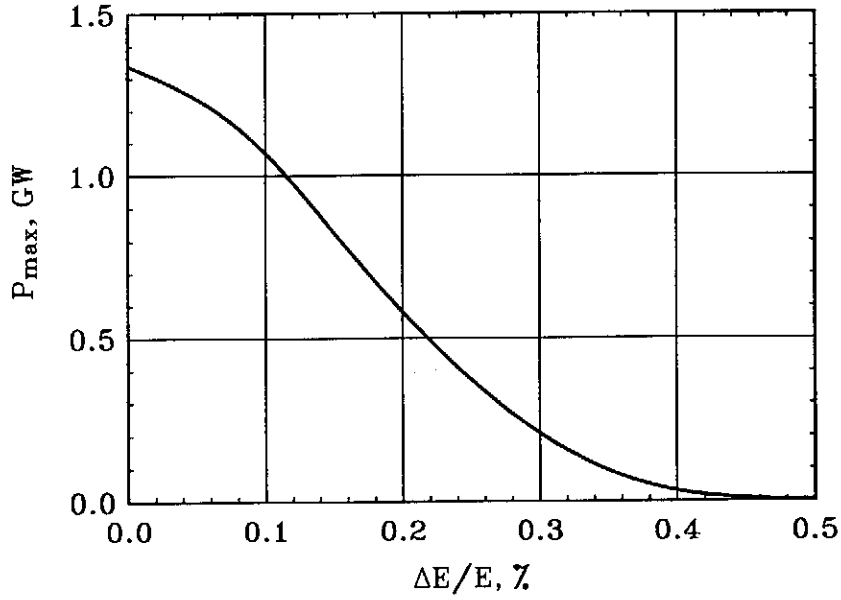

Fig. 7. Dependence of the maximal output power on the value of the energy spread.

(a) 6 nm option. Here $\epsilon_n = 10^{-4}$ cm rad.

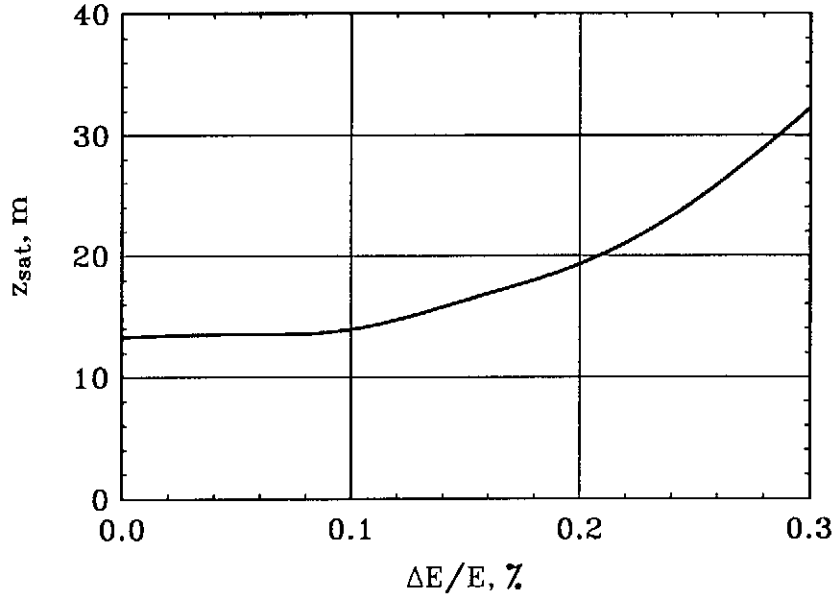

(b) 70 nm option. Here $\epsilon_n = 2 \times 10^{-4}$ cm rad.

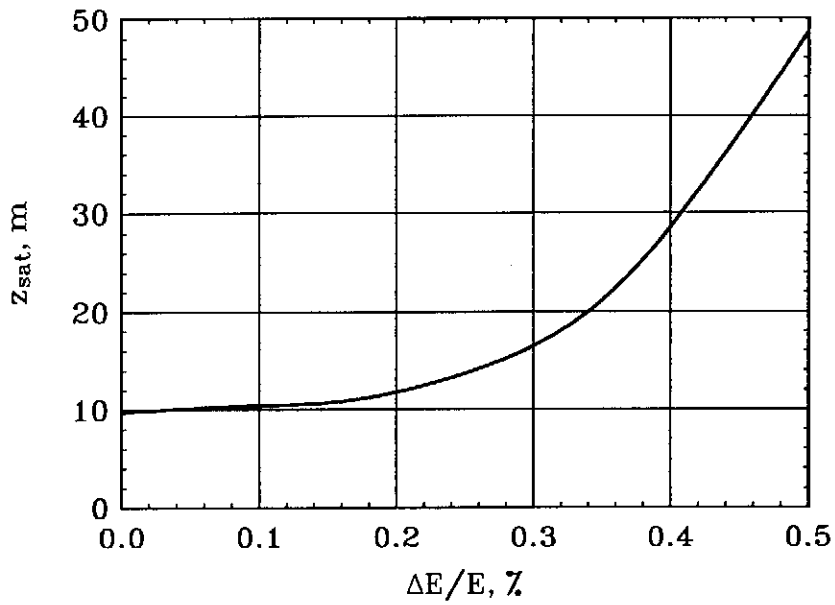

Fig. 8. Saturation length versus energy spread.

(a) 6 nm option. (1): $I = 2.5$ kA, (2): $I = 2$ kA, (3): $I = 1.5$ kA, (4): $I = 1$ kA. Here $\epsilon_n = 10^{-4}$ cm rad, $\sigma_E/\mathcal{E} = 0.1\%$.

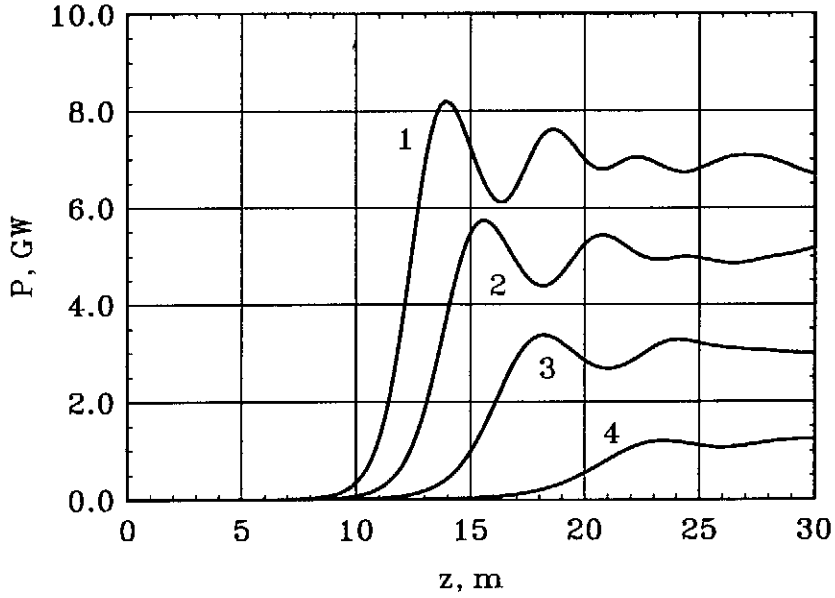

(b) 70 nm option. (1): $I = 600$ A, (2): $I = 480$ A, (3): $I = 360$ A, (4): $I = 240$ A. Here $\epsilon_n = 2 \times 10^{-4}$ cm rad, $\sigma_E/\mathcal{E} = 0.17\%$.

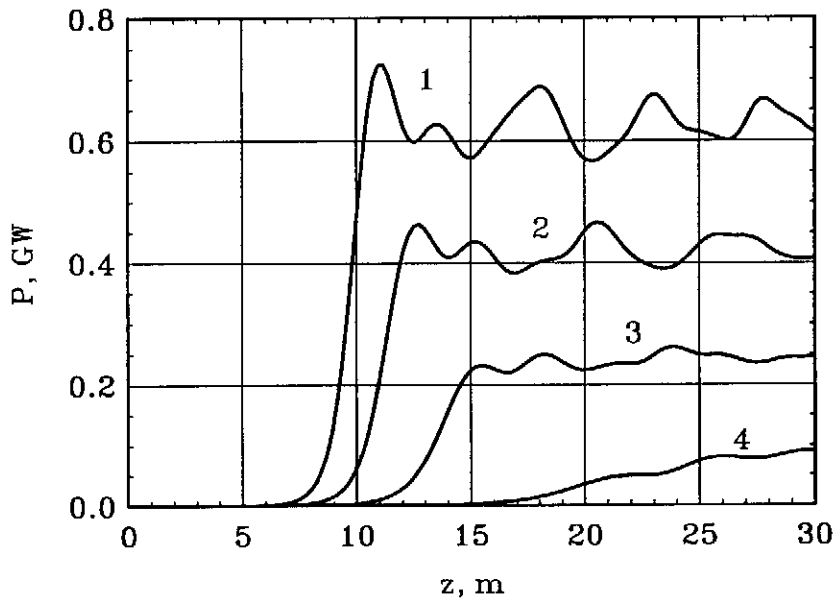

Fig. 9. Dependence of the output power on the ondulator length.

(a) 6 nm option. (1): Beam current distribution, (2): Power distribution at $z = 14$ m, (3): Power distribution at $z = 20$ m. Here $\epsilon_n = 10^{-4}$ cm rad, $\sigma_E/\mathcal{E} = 0.1$ % .

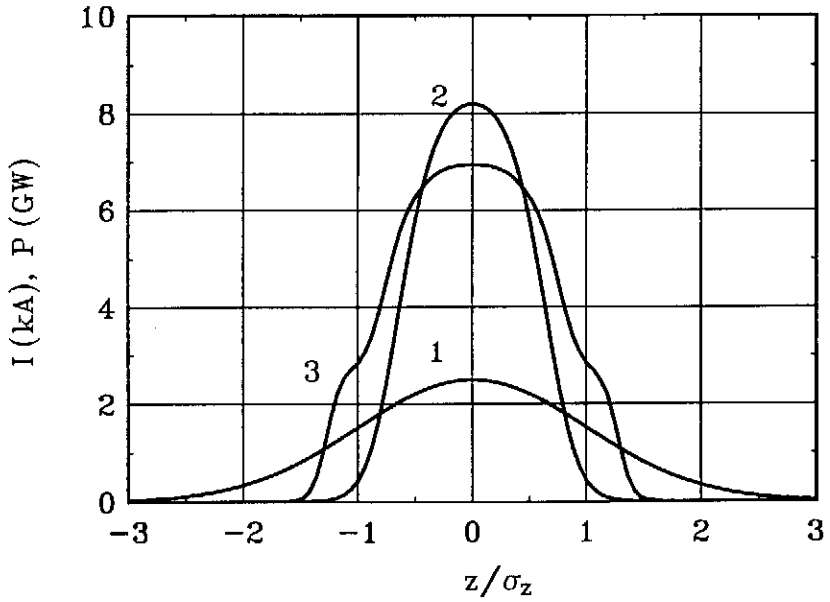

(b) 70 nm option. (1): Beam current distribution, (2): Power distribution at z = 11 m, (3): Power distribution at z = 15 m. Here $\epsilon_n = 2 \times 10^{-4}$ cm rad, $\sigma_E/\mathcal{E} = 0.17\%$.

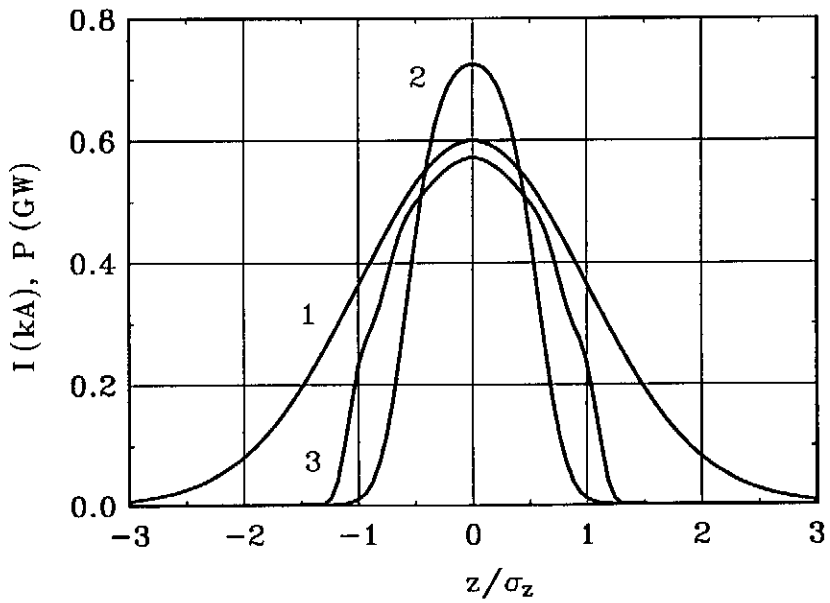

Fig. 10. Power distribution along the beam.

(a) 6 nm option. Here $\epsilon_n = 10^{-4}$ cm rad, $\sigma_E/\mathcal{E} = 0.1\%$.

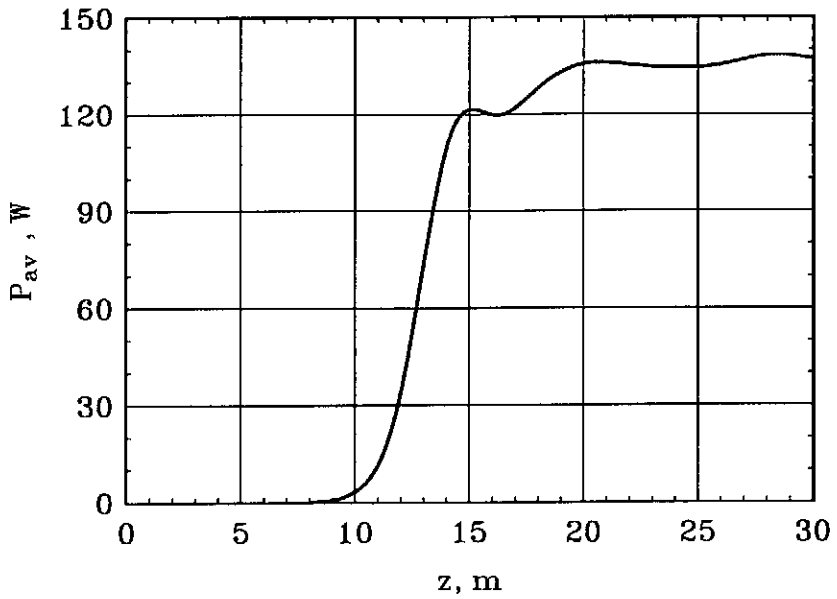

(b) 70 nm option. Here $\epsilon_n = 2 \times 10^{-4}$ cm rad, $\sigma_E/\mathcal{E} = 0.17\%$.

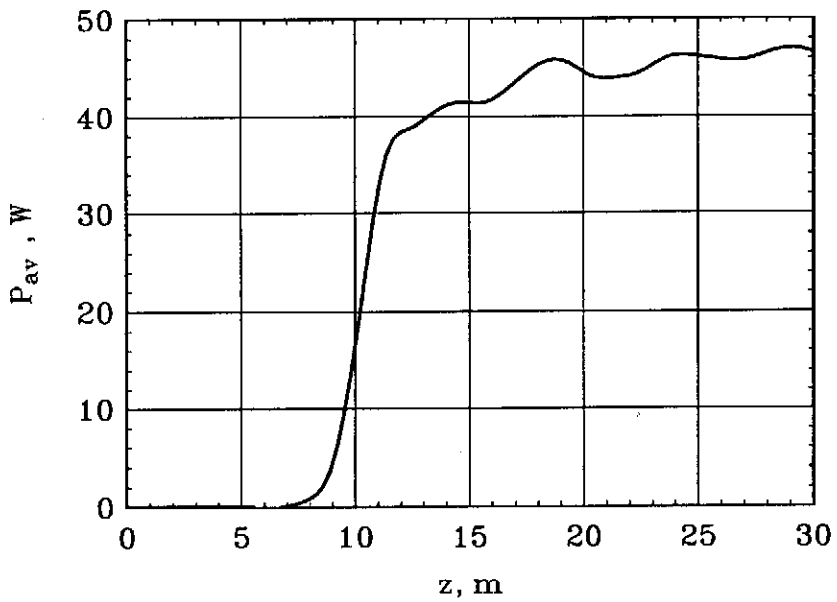

Fig. 11. Dependence of the average power on the undulator length.

(a) 6 nm option. Here $\epsilon_n = 10^{-4}$ cm rad, $\sigma_E/\mathcal{E} = 0.1\%$ and $z = 14$ m (saturation point).

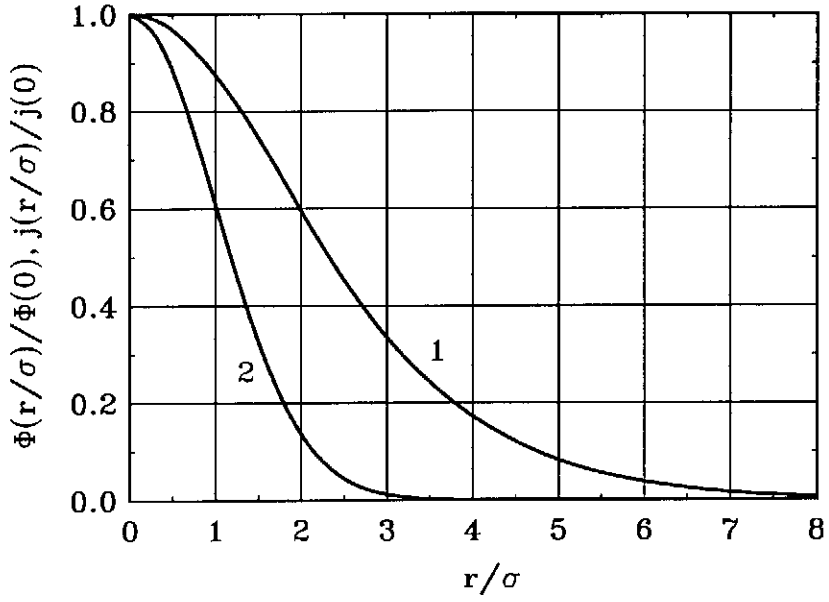

(b) 70 nm option. Here $\epsilon_n = 2 \times 10^{-4}$ cm rad, $\sigma_E/\mathcal{E} = 0.17\%$ and $z = 11$ m (saturation point).

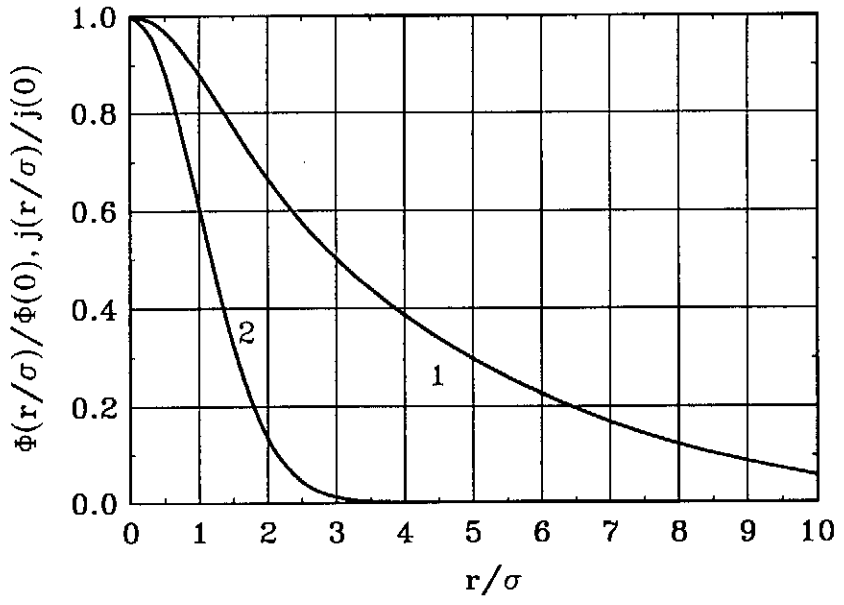

Fig. 13. Distribution of the radiation field (1) inside the undulator (curve (2) is the beam current density).

(a) 6 nm option. Here $\epsilon_n = 10^{-4}$ cm rad, $\sigma_E/\mathcal{E} = 0.1\%$ and $z = 14$ m (saturation point).

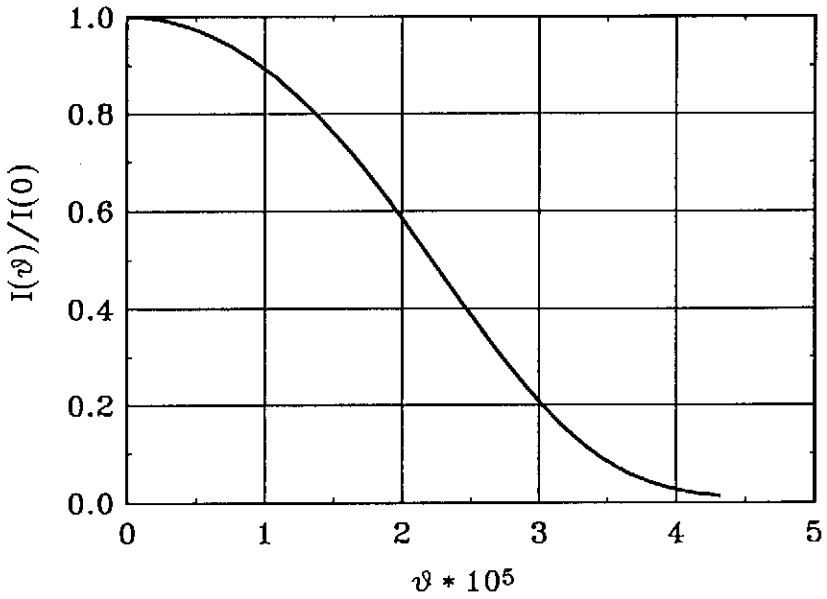

(b) 70 nm option. Here $\epsilon_n = 2 \times 10^{-4}$ cm rad, $\sigma_E/\mathcal{E} = 0.17\%$ and $z = 11$ m (saturation point).

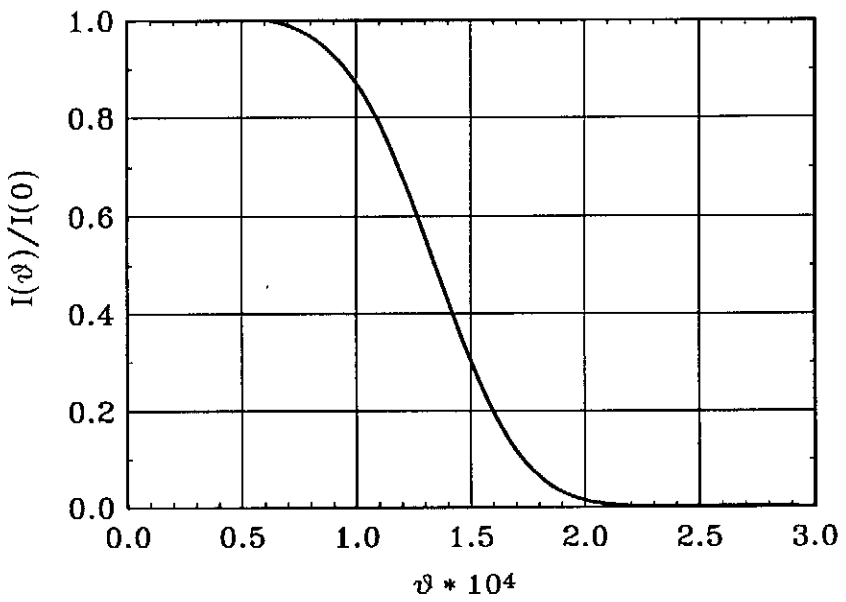

Fig. 14. Directivity diagram of radiation in the Fraunhofer diffraction zone.

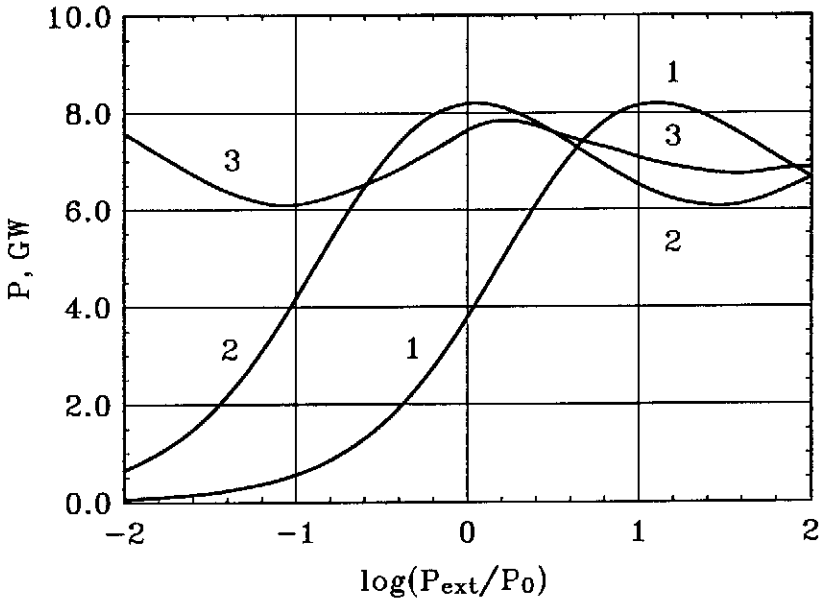

Fig. 15. 6 nm option. Dependence of the output power versus input power. (1): $z = 12$ m, (2): $z = 14$ m, (3): $z = 18$ m. Here $\epsilon_n = 10^{-4}$ cm rad, $\sigma_E/\mathcal{E} = 0.1$ % and $P_0 = 1$ kW.